FISFVIER

Contents lists available at ScienceDirect

Journal of Computational Physics

journal homepage: www.elsevier.com/locate/jcp





Linear relaxation method with regularized energy reformulation for phase field models

Jiansong Zhang ^a, Xinxin Guo ^a, Maosheng Jiang ^b, Tao Zhou ^c, Jia Zhao ^{d,*}

- ^a Department of Applied Mathematics, China University of Petroleum, Qingdao 266580, PR China
- ^b School of Mathematics and Statistics, Qingdao University, Qingdao 266071, PR China
- c Institute of Computational Mathematics and Scientific/Engineering Computing, Academy of Mathematics and Systems Science, Chinese Academy of Sciences, Beijing, 100190, PR China
- d Department of Mathematics and Statistics, Binghamton University, Binghamton, NY, 13902, USA

ARTICLE INFO

Keywords: Linear relaxation Energy reformulation Phase field models Energy stable Molecular beam epitaxy (MBE) model Phase-field crystal (PFC) model

ABSTRACT

In this paper, we establish a novel linear relaxation method with regularized energy reformulation for phase field models, which we name the RRER method. We employ the molecular beam epitaxy (MBE) model and the phase-field crystal (PFC) model as test beds, along with several coupled phase field models, to illustrate the concept. Our proposed RRER strategy is applicable to a broad class of phase field models that can be derived through energy variation. The RRER method consists of two major steps. First, we introduce regularized auxiliary variables to reformulate the original phase field models into equivalent forms where the free energy is transformed under the auxiliary variables. Then, we discretize the reformulated PDE model under these variables on a staggered time mesh for the phase field models. We incorporate the energy reformulation idea in the first step and the linear relaxation concept in the second step to derive a general numerical algorithm for phase field models that is linear and second-order accurate. Our approach differs from the classical invariant energy quadratization (IEQ) and scalar auxiliary variable (SAV) approaches, as we don't need to take time derivatives for the auxiliary variables. The resulting schemes are linear, i.e., only linear algebraic systems need to be solved at each time step. Rigorous theoretical analysis demonstrates that these resulting schemes satisfy the modified discrete energy dissipation laws and preserve the discrete mass conservation for the PFC and MBE models. Furthermore, we present numerical results to demonstrate the effectiveness of our method in solving phase field models.

1. Introduction

The phase field method has been widely used to solve interfacial problems. Instead of explicitly tracking the interface, the phase field method introduces phase variables and the evolution of interfaces is embedded in the evolution of the phase field variables, which are typically governed by PDEs. Those PDEs are named phase field PDE models. Due to its simplicity and direct physical interpretation, the phase field method has gained widespread recognition and been frequently utilized across various fields. Notable applications span hydrodynamics, material sciences, biology, and image processing. See [3–9].

https://doi.org/10.1016/j.jcp.2024.113225

Received 11 November 2023; Received in revised form 14 June 2024; Accepted 23 June 2024

^{*} Corresponding author.

E-mail address: jiazhao@binghamton.edu (J. Zhao).

In general, the phase field PDE model can be described by a triple (ϕ, \mathcal{G}, E) and derived from the energy variational approach, as shown in the generic form

$$\frac{\partial \phi}{\partial t} = -\mathcal{G} \frac{\delta E(\phi)}{\delta \phi},\tag{1.1}$$

where $\phi = \phi(\mathbf{x}, t)$ denotes the phase variable function, \mathcal{G} is a semi-positive definite mobility operator, $E(\phi)$ is the free energy functional, and $\frac{\delta E(\phi)}{\delta \phi}$ is the variational derivative, known as the chemical potential. With proper boundary conditions, saying the boundary integrals vanish, it is easily seen that the phase field model has an energy dissipation property as

$$\frac{d}{dt}E(\phi) = (\frac{\delta E}{\delta \phi}, \frac{\partial \phi}{\partial t}) = -(\frac{\delta E}{\delta \phi}, \mathcal{G}\frac{\delta E}{\delta \phi}) \le 0, \tag{1.2}$$

where the inner product is defined as $(f,g) = \int_{\Omega} fg d\mathbf{x}$, $\forall f,g \in L^2(\Omega)$ with Ω the domain.

In practical application, when the free energy $E(\phi)$ and the mobility operator \mathcal{G} are given, a specific phase field model can be derived from (1.1). For example, if the triple is taken as

$$(\phi, \mathcal{G}, E) := \left(\phi, \quad I, \quad \int\limits_{\Omega} \left(\frac{\epsilon^2}{2} (\nabla \phi)^2 + F(\phi)\right) d\mathbf{x}\right),\tag{1.3}$$

we get the Allen-Cahn (AC) equation that can be written as follows

$$\frac{\partial \phi}{\partial t} = \epsilon^2 \Delta \phi - f(\phi),$$

where $f(\phi) = F'(\phi)$. Meanwhile, if the triple is taken as

$$(\phi, \mathcal{G}, E) := \left(\phi, -\lambda \Delta, \int_{\Omega} \left(\frac{\epsilon^2}{2} (\nabla \phi)^2 + F(\phi)\right) d\mathbf{x}\right), \tag{1.4}$$

where only the mobility operator in (1.3) is replaced, we arrive at a different phase field model. It is the well-known Cahn-Hilliard (CH) equation that is written as

$$\frac{\partial \phi}{\partial t} = \lambda \Delta (-\epsilon^2 \Delta \phi + f(\phi)).$$

Furthermore, if we take a different triple by replacing the free energy in (1.4) as

$$(\phi, \mathcal{G}, E) := \Big(\phi, \quad -\lambda \Delta, \quad \int\limits_{\Omega} \Big(\frac{1}{2}\phi(a_0 + \Delta)^2 \phi + F(\phi)\Big) d\mathbf{x}\Big),$$

the phase field crystal (PFC) equation can be derived, which is given as

$$\frac{\partial \phi}{\partial t} = \lambda \Delta ((a_0 + \Delta)^2 \phi + f(\phi)).$$

Or if we replace the free energy in (1.3) as below

$$(\phi, \mathcal{G}, E) := \left(\phi, I, \int_{\Omega} \left(\frac{\epsilon^2}{2} (\Delta \phi)^2 + F(\nabla \phi)\right) d\mathbf{x}\right),$$

the molecular beam epitaxy (MBE) equation can be derived

$$\frac{\partial \phi}{\partial t} = -\epsilon^2 \Delta^2 \phi + \nabla \cdot f(\nabla \phi).$$

Many variants for the mobility operators and the free energies lead to different phase field models. Interested readers can refer to [1,2] and the references therein.

Given the complexity and nonlinearity of the phase field equations, their analytical solutions are generally not known, making the numerical method a handy tool for exploring the dynamics governed by the phase field models. Unfortunately, even though the phase field models are easy to formulate and their results are easy to interpret, the phase field PDEs are not easy to solve numerically, mainly due to the stiffness in the nonlinear terms that have strict requirements on the time marching steps. Furthermore, given the intrinsic energy dissipation property as shown in (1.2), the numerical schemes should also preserve the energy dissipation law to maintain the embedded thermodynamics laws in the phase field PDEs during numerical simulations. Such numerical schemes are known as energy stable. If the energy stability is guaranteed without any restriction on the time step sizes, the numerical schemes are known as unconditionally energy stable. In other words, designing numerical schemes that preserve the energy dissipation law at the discrete level is especially desirable for solving the phase field PDEs. One reason is that preserving the energy dissipation property plays a crucial role in capturing the correct long time dynamics of the system. The other reason is that the unconditional energy stability provides flexibility for dealing with the stiffness issue in phase field models. Meanwhile, some other quantities, such as mass conservation, shall also not be violated numerically, which puts extra demands on numerical algorithm design for the phase field models.

Many experts and scholars are interested in developing unconditional energy-stable schemes, and a lot of literature has been published on numerical methods for the phase field models. Some popular and widely used methods include convex splitting approach [10–13], exponential time differencing (ETD) approach [14–16], invariant energy quadratization (IEQ) approach [17–21], scalar auxiliary variable (SAV) approach [22–26], Lagrange multiplier approach [27] and supplementary variable method [40]. The convex splitting method splits the nonlinear terms of free energy into the subtraction of two convex functions and is stable and uniquely solvable. The stabilization method [28] displays the nonlinear term and adds a regularization term to ensure stability, but it is usually limited to first-order accuracy. The invariant energy quadratization is a generalization of the method of Lagrange multipliers and usually leads to a coupled system with time-dependent coefficients. The scalar auxiliary variable method keeps the advantages of the invariant energy quadratization approach but usually leads to a decoupled system with constant coefficients. Recently, Jiang et al. proposed a linear relaxation scheme that is second-order and unconditionally energy stable in [32]. The key idea in developing the linear relaxation scheme is to discretize the equation on a staggered grid.

In this work, our primary contribution is to propose a new class of numerical schemes for phase field models by embracing the merits of relaxation techniques and regularized energy reformulation strategies. Using the MBE and PFC models as examples, the resulting semi-discrete schemes are linear and unconditionally energy stable. Unlike the IEQ-type and SAV-type methods, we do not need to take the time derivative of the auxiliary variables, making the scheme more consistent with the original differential equation systems. These schemes are of second-order accuracy in time and unconditionally energy stable, so they can significantly improve computational efficiency. Rigorous stability analysis and mass conservation are also considered for the two linear regularized energy reformulation approaches of MBE and PFC models. Both theoretical results and numerical examples suggest our methods are unconditionally energy stable and mass conservative for conservative phase field models. Finally, we provide some numerical examples to perform numerical simulations of coarsening dynamics.

The rest of this paper is organized as follows. Firstly, we give the regularized energy reformulation approach for the general phase field model in Section 2. Then, we present the linear regularized energy reformulation approaches for various models. Meanwhile, we prove that these schemes are unconditionally energy stable with the modified discrete energy forms and keep mass conservation. In section 3, we present some numerical examples with the proposed methods. Finally, conclusion remarks are provided in Section 4.

2. Relaxation method with regularized energy reformulation

First, we introduce some notations that will be frequently used in this paper. Throughout this paper, we consider the regular domain $\Omega \in \mathbb{R}^d$ (where d=2,3) with periodic boundary conditions. We use the notation of the inner product $(f,g) = \int_{\Omega} f g d\mathbf{x}, \forall f,g \in L^2(\Omega)$, and the induced norm $||f|| = \sqrt{(f,f)}$. Our results can be directly extended to solve problems with other physical boundary conditions. For simplicity, this paper only considers periodic boundary conditions.

2.1. Regularized energy reformulation for phase field models

To illustrate our method, we start with a simplified free energy

$$E(\phi) = \frac{1}{2}(\mathcal{L}\phi, \phi) + (F(\phi), 1),$$
 (2.1)

where \mathcal{L} is a linear operator. Then, we can rewrite the general phase field model of (1.1) in the following equivalent form:

$$\frac{\partial \phi}{\partial t} = -G(\mathcal{L}\phi + F'(\phi)),\tag{2.2}$$

with the energy dissipation law

$$\frac{d}{dt}E(\phi) = \left(\frac{\delta E}{\delta \phi}, \frac{\partial \phi}{\partial t}\right) = -\left(\mathcal{L}\phi + F'(\phi), \mathcal{G}(\mathcal{L}\phi + F'(\phi))\right) \le 0,$$

given that $G \ge 0$, i.e., G is a semi positive definite operator.

Next, we briefly revisit the regularized energy quadratization idea. Introducing the regularized auxiliary variable

$$q = \sqrt{4(F(\phi) + C_0)} - \gamma,$$
 (2.3)

where C_0 is a constant such that $F(\phi) + C_0 \ge 0$ and γ is a stabilization parameter. From the above equation, we can get

$$F(\phi) = \frac{1}{4}q^2 + \frac{1}{2}\gamma q + \frac{\gamma^2}{4} - C_0.$$

Differentiating $F(\phi)$ and q with respect to ϕ , we get

$$F'(\phi) = \frac{1}{2}qq' + \frac{\gamma}{2}q', \quad q' = \frac{dq}{d\phi}.$$

Hence, we have the following equivalent form of (2.2)

$$\begin{cases} \frac{\partial \phi}{\partial t} = -G\mu, \\ \mu = \mathcal{L}\phi + \frac{1}{2}qq' + \frac{\gamma}{2}q', \\ q = \sqrt{4(F(\phi) + C_0)} - \gamma. \end{cases}$$
(2.4)

Define the modified energy $\hat{E}(\phi, q)$ as

$$\hat{E}(\phi, q) = \frac{1}{2} (\mathcal{L}\phi, \phi) + \left(\frac{1}{4}q^2 + \frac{1}{2}\gamma q + \frac{\gamma^2}{4} - C_0, 1\right). \tag{2.5}$$

The reformulated model (2.4) has the modified energy law

$$\begin{split} \frac{d}{dt}\hat{E}(\phi,q) &= \left(\frac{\delta\hat{E}}{\delta\phi},\frac{\partial\phi}{\partial t}\right) + \left(\frac{\delta\hat{E}}{\delta q},q'\frac{\partial\phi}{\partial t}\right) \\ &= \left(\frac{\delta\hat{E}}{\delta\phi},\frac{\partial\phi}{\partial t}\right) + \left(\frac{1}{2}q + \frac{1}{2}\gamma,q'\frac{\partial\phi}{\partial t}\right) \\ &= -\left(\mathcal{L}\phi + \frac{1}{2}qq' + \frac{\gamma}{2}q',\mathcal{G}\left(\mathcal{L}\phi + \frac{1}{2}qq' + \frac{\gamma}{2}q'\right)\right) \leq 0. \end{split}$$

Remark 2.1. We emphasize that the reformulation in (2.4) is different from the IEQ and SAV approaches [17,18,22,23] since we don't take time derivatives for the auxiliary variables in (2.3) that introduces truncation errors during numerical computations.

In the following sections, we will give the linear regularized energy reformulation approaches for the MBE and PFC models from the viewpoint of practical implementation.

2.2. RRER method for the molecular beam epitaxy (MBE) model

Consider the free energy

$$E(\phi) = \int_{\Omega} \left(\frac{\epsilon^2}{2} (\Delta \phi)^2 + \frac{1}{4} (|\nabla \phi|^2 - 1)^2 \right) d\mathbf{x},$$

and the mobility operator G = I, where I is the identity operator. Then the phase field model in (1.1) is specified as

$$\phi_{\epsilon} = -\epsilon^2 \Delta^2 \phi + \nabla \cdot ((|\nabla \phi|^2 - 1)\nabla \phi), \tag{2.6}$$

which is the so-called molecular beam epitaxy model with slope selection [29-31].

With the periodic boundary condition or any other proper boundary condition that can satisfy the flux-free condition at the boundary $\partial \phi/\partial \mathbf{n}|_{\partial\Omega} = 0$ and $\partial \Delta \phi/\partial \mathbf{n}|_{\partial\Omega} = 0$, we have the mass conservation property

$$\frac{d}{dt} \int_{\Omega} \phi(\mathbf{x}, t) d\mathbf{x} = 0,$$

where \mathbf{n} is the outward normal on the boundary $\partial\Omega$. So, proposing a discrete numerical scheme that preserves energy dissipation and keeps mass conservation simultaneously is desirable.

Next, we will establish our numerical scheme for the MBE model with slope selection. We introduce an auxiliary variable

$$q = |\nabla \phi|^2 - 1 - \gamma, \tag{2.7}$$

where $\gamma > 0$ is a stabilization parameter. Substituting (2.7) into (2.6), we have

$$\phi_{t} = -\epsilon^{2} \Delta^{2} \phi + \nabla \cdot (a \nabla \phi) + \gamma \Delta \phi.$$

Set $g = \Delta \phi$. Then we can get the following equivalent form of (2.6)

$$\begin{cases} \phi_t = -\epsilon^2 \Delta g + \nabla \cdot (q \nabla \phi) + \gamma g, \\ g = \Delta \phi, \\ q = |\nabla \phi|^2 - 1 - \gamma, \end{cases}$$
 (2.8)

where the corresponding energy functional $E(\phi)$ is reformulated as follows:

$$\hat{E}(\phi,q) = \frac{\epsilon^2}{2} \|\Delta\phi\|^2 + \frac{\gamma}{2} \|\nabla\phi\|^2 + \frac{1}{2} (q(|\nabla\phi|^2 - 1 - \gamma), 1) - \frac{1}{4} \|q\|^2 - \frac{2\gamma + \gamma^2}{4} |\Omega|,$$

where $|\Omega| = \int_{\Omega} d\mathbf{x}$.

Remark 2.2. We emphasize that the modified energy $E(\phi, q)$ for the transformed model (2.8) is equivalent to the original energy $E(\phi)$. We can derive the equivalence as below.

$$\begin{split} E(\phi) &= \int_{\Omega} (\frac{\epsilon^2}{2} (\Delta \phi)^2 + \frac{1}{4} (|\nabla \phi|^2 - 1)^2) d\mathbf{x} \\ &= \int_{\Omega} (\frac{\epsilon^2}{2} (\Delta \phi)^2 + \frac{1}{4} (q + \gamma)^2) d\mathbf{x} \\ &= \int_{\Omega} (\frac{\epsilon^2}{2} (\Delta \phi)^2 + \frac{1}{4} q^2 + \frac{\gamma}{2} (|\nabla \phi|^2 - 1 - \gamma) + \frac{1}{4} r^2) d\mathbf{x} \\ &= \int_{\Omega} (\frac{\epsilon^2}{2} (\Delta \phi)^2 + \frac{1}{4} q^2 + \frac{\gamma}{2} |\nabla \phi|^2 - \frac{2\gamma + \gamma^2}{4}) d\mathbf{x} \\ &= \frac{\epsilon^2}{2} ||\Delta \phi||^2 + \frac{\gamma}{2} ||\nabla \phi||^2 + \frac{1}{2} (q(|\nabla \phi|^2 - 1 - \gamma), 1) - \frac{1}{4} ||q||^2 - \frac{2\gamma + \gamma^2}{4} |\Omega| \\ &= \hat{E}(\phi, q). \end{split}$$

Therefore, in the following part of this section, we will present a numerical approximation for the system (2.8) and show the numerical scheme preserves the properties of mass conservation and energy dissipation. To give the time-discrete scheme of system (2.8), we denote $\delta t > 0$ the time step. Now, we provide the time-discretize formulation of (2.8) based on the Crank-Nicolson scheme.

Algorithm 1. Assume that $(\phi^n, q^{n-\frac{1}{2}})$ are already calculated with $n \ge 1$. Then we compute $(\phi^{n+1}, g^{n+\frac{1}{2}}, q^{n+\frac{1}{2}})$ from the following temporal discrete system:

(a)
$$\frac{\phi^{n+1} - \phi^n}{\delta t} = -\epsilon^2 \Delta g^{n+\frac{1}{2}} + \nabla \cdot (q^{n+\frac{1}{2}} \nabla \frac{\phi^{n+1} + \phi^n}{2}) + \gamma g^{n+\frac{1}{2}},$$
(b)
$$g^{n+\frac{1}{2}} = \Delta \frac{\phi^{n+1} + \phi^n}{2},$$
(c)
$$\frac{q^{n+\frac{1}{2}} + q^{n-\frac{1}{2}}}{2} = |\nabla \phi^n|^2 - 1 - \gamma.$$
(2.9)

Remark 2.3. Algorithm 1 is of second-order accuracy in time. In practical implementation, we can compute $(\phi^1, q^{\frac{1}{2}})$ using the following numerical approximation

$$\begin{split} q^{\frac{1}{2}} &= |\nabla \phi^0|^2 - 1 - \gamma, \\ g^{\frac{1}{2}} &= \Delta \frac{\phi^1 + \phi^0}{2}, \\ \frac{\phi^1 - \phi^0}{\delta t} &= -\epsilon^2 \Delta g^{\frac{1}{2}} + \nabla \cdot (q^{\frac{1}{2}} \nabla \frac{\phi^1 + \phi^0}{2}) + \gamma g^{\frac{1}{2}}. \end{split}$$

Theorem 2.4. Algorithm 1 preserves the property of total mass conservation.

Proof. Multiplying (2.9)(a) by δt and integrating it over Ω , we have

$$\int_{\Omega} \phi^{n+1} d\mathbf{x} - \int_{\Omega} \phi^{n} d\mathbf{x} = \delta t \int_{\Omega} \left(-e^{2} \Delta g^{n+\frac{1}{2}} + \nabla \cdot (q^{n+\frac{1}{2}} \nabla \frac{\phi^{n+1} + \phi^{n}}{2}) + \gamma g^{n+\frac{1}{2}} \right) d\mathbf{x}.$$
 (2.10)

Integrating (2.9)(b) over Ω , we can get

$$\int_{\Omega} g^{n+\frac{1}{2}} d\mathbf{x} = \int_{\Omega} \Delta \frac{\phi^{n+1} + \phi^n}{2} d\mathbf{x}.$$
 (2.11)

Substituting (2.11) into (2.10) and using Green's formula, we get

$$\int_{\Omega} \phi^{n+1} d\mathbf{x} = \int_{\Omega} \phi^n d\mathbf{x},$$

which implies that Algorithm 1 is mass conservative. \Box

Furthermore, we have the following energy stability theorem.

Theorem 2.5. Algorithm 1 is unconditionally energy stable. In particular, Algorithm 1 satisfies the following energy dissipation law: for any $n \ge 1$,

$$\hat{E}^{n+1}(\phi^{n+1}, q^{n+\frac{1}{2}}) - \hat{E}^{n}(\phi^{n}, q^{n-\frac{1}{2}}) = -\delta t \|\mu^{n+\frac{1}{2}}\|^{2} \le 0,$$

where the chemical potential and modified energy are given as

$$\begin{split} &\mu^{n+\frac{1}{2}} = \epsilon^2 \Delta g^{n+\frac{1}{2}} - \nabla \cdot (q^{n+\frac{1}{2}} \nabla \frac{\phi^{n+1} + \phi^n}{2}) - \gamma g^{n+\frac{1}{2}}, \\ &\hat{E}^{n+1}(\phi^{n+1}, q^{n+\frac{1}{2}}) = \frac{\epsilon^2}{2} \|\Delta \phi^{n+1}\|^2 + \frac{\gamma}{2} \|\nabla \phi^{n+1}\|^2 + \frac{1}{2} (q^{n+\frac{1}{2}} (|\nabla \phi^{n+1}|^2 - 1 - \gamma), 1) - \frac{1}{4} \|q^{n+\frac{1}{2}}\|^2 - \frac{2\gamma + \gamma^2}{4} |\Omega|. \end{split}$$

Proof. Multiplying (2.9)(a) by $\delta t \mu^{n+\frac{1}{2}}$ and integrating it over Ω , we can obtain immediately

$$(\phi^{n+1} - \phi^n, \epsilon^2 \Delta g^{n+\frac{1}{2}} - \nabla \cdot (q^{n+\frac{1}{2}} \nabla \frac{\phi^{n+1} + \phi^n}{2}) - \gamma g^{n+\frac{1}{2}}) = -\delta t \|\mu^{n+\frac{1}{2}}\|^2.$$

This can be simplified as

$$\epsilon^{2}(\phi^{n+1} - \phi^{n}, \Delta g^{n+\frac{1}{2}}) - \gamma(\phi^{n+1} - \phi^{n}, g^{n+\frac{1}{2}}) + \frac{1}{2}(q^{n+\frac{1}{2}}(|\nabla \phi^{n+1}|^{2} - |\nabla \phi|^{2}), 1) = -\delta t \|\mu^{n+\frac{1}{2}}\|^{2}. \tag{2.12}$$

Note that

$$(q^{n+\frac{1}{2}}(|\nabla \phi^{n+1}|^2 - |\nabla \phi^n|^2), 1) = (q^{n+\frac{1}{2}}(|\nabla \phi^{n+1}|^2 - |\nabla \phi^n|^2), 1) + (q^{n-\frac{1}{2}}(|\nabla \phi^n|^2 - |\nabla \phi^n|^2), 1)$$

$$= (q^{n+\frac{1}{2}}(|\nabla \phi^{n+1}|^2 - 1 - \gamma), 1) - (q^{n-\frac{1}{2}}(|\nabla \phi^n|^2 - 1 - \gamma), 1)$$

$$- ((q^{n+\frac{1}{2}} - q^{n-\frac{1}{2}})(|\nabla \phi^n|^2 - 1 - \gamma), 1).$$
(2.13)

Multiplying (2.9)(c) by $q^{n+\frac{1}{2}}-q^{n-\frac{1}{2}}$ and integrating it over Ω , we get

$$\frac{1}{2}(\|q^{n+\frac{1}{2}}\|^2 - \|q^{n-\frac{1}{2}}\|^2) = ((q^{n+\frac{1}{2}} - q^{n-\frac{1}{2}})(|\nabla \phi^n|^2 - 1 - \gamma), 1). \tag{2.14}$$

Substituting (2.14) into (2.13), we have

$$(q^{n+\frac{1}{2}}(|\nabla \phi^{n+1}|^2 - |\nabla \phi^n|^2), 1) = (q^{n+\frac{1}{2}}(|\nabla \phi^{n+1}|^2 - 1 - \gamma), 1) - (q^{n-\frac{1}{2}}(|\nabla \phi^n|^2 - 1 - \gamma), 1) - \frac{1}{2}(||q^{n+\frac{1}{2}}||^2 - ||q^{n-\frac{1}{2}}||^2).$$

$$(2.15)$$

In addition, multiplying (2.9)(b) by $e^2 \Delta(\phi^{n+1} - \phi^n)$ and integrating them over Ω , we have

$$\frac{\epsilon^2}{2}(\|\Delta\phi^{n+1}\|^2 - \|\Delta\phi^n\|^2) = \epsilon^2(g^{n+\frac{1}{2}}, \Delta(\phi^{n+1} - \phi^n)) = \epsilon^2(\Delta g^{n+\frac{1}{2}}, \phi^{n+1} - \phi^n), \tag{2.16}$$

where we have used Green's formula in the last equation.

Meantime, integrating (2.9)(b) with $\phi^{n+1} - \phi^n$ over the domain, we get

$$(g^{n+\frac{1}{2}},\phi^{n+1}-\phi^n) = -\frac{1}{2}(\|\nabla\phi^{n+1}\|^2 - \|\nabla\phi^n\|^2). \tag{2.17}$$

Substituting (2.15), (2.16) and (2.17) into (2.12), we can obtain

$$\frac{\epsilon^{2}}{2} \|\Delta \phi^{n+1}\|^{2} + \frac{\gamma}{2} \|\nabla \phi^{n+1}\|^{2} + \frac{1}{2} (q^{n+\frac{1}{2}} (|\nabla \phi^{n+1}|^{2} - 1 - \gamma), 1) - \frac{1}{4} \|q^{n+\frac{1}{2}}\|^{2}
- \frac{\epsilon^{2}}{2} \|\Delta \phi^{n}\|^{2} - \frac{\gamma}{2} \|\nabla \phi^{n}\|^{2} - \frac{1}{2} (q^{n-\frac{1}{2}} (|\nabla \phi^{n}|^{2} - 1 - \gamma), 1) + \frac{1}{4} \|q^{n-\frac{1}{2}}\|^{2}
= -\delta t \|\mu^{n+\frac{1}{2}}\|^{2} \le 0.$$
(2.18)

Therefore, we can get

$$\hat{E}^{n+1}(\phi^{n+1}, q^{n+\frac{1}{2}}) - \hat{E}^{n}(\phi^{n}, q^{n-\frac{1}{2}}) = -\delta t \|\mu^{n+\frac{1}{2}}\|^{2} \le 0,$$

which shows that Algorithm 1 is unconditionally energy stable with respect to the modified discrete energy.

Remark 2.6. We provide an intuitive explanation of the connections between modified and original energy. Notice the fact,

$$\begin{split} E(\phi^{n+1}) \approx & \hat{E}(\phi^{n+1}, q^{n+1}) \\ &= \frac{\epsilon^2}{2} \|\Delta \phi^{n+1}\|^2 + \frac{\gamma}{2} \|\nabla \phi^{n+1}\|^2 + \frac{1}{2} (q^{n+1} (|\nabla \phi^{n+1}|^2 - 1 - \gamma), 1) - \frac{1}{4} \|q^{n+1}\|^2 - \frac{2\gamma + \gamma^2}{4} |\Omega| \\ &= \frac{\epsilon^2}{2} \|\Delta \phi^{n+1}\|^2 + \frac{\gamma}{2} \|\nabla \phi^{n+1}\|^2 + \frac{1}{2} (q^{n+\frac{1}{2}} (|\nabla \phi^{n+1}|^2 - 1 - \gamma), 1) - \frac{1}{4} \|q^{n+\frac{1}{2}}\|^2 - \frac{2\gamma + \gamma^2}{4} |\Omega| \\ &+ \frac{1}{2} (q^{n+1} (|\nabla \phi^{n+1}|^2 - 1 - \gamma), 1) - \frac{1}{2} (q^{n+\frac{1}{2}} (|\nabla \phi^{n+1}|^2 - 1 - \gamma), 1) - \frac{1}{4} \|q^{n+1}\|^2 + \frac{1}{4} \|q^{n+\frac{1}{2}}\|^2 \\ &= \hat{E}^{n+1} (\phi^{n+1}, q^{n+\frac{1}{2}}) + \frac{1}{2} (q^{n+1} (|\nabla \phi^{n+1}|^2 - 1 - \gamma), 1) \\ &- \frac{1}{2} (q^{n+\frac{1}{2}} (|\nabla \phi^{n+1}|^2 - 1 - \gamma), 1) - \frac{1}{4} \|q^{n+1}\|^2 + \frac{1}{4} \|q^{n+\frac{1}{2}}\|^2 \\ &\approx \hat{E}^{n+1} (\phi^{n+1}, q^{n+\frac{1}{2}}) + \frac{1}{4} (q^{n+1} - q^{n+\frac{1}{2}}, q^{n+1} - q^{n+\frac{1}{2}}). \end{split}$$

The approximations above are all second-order accurate in time. Therefore, the modified energy is, in fact, a second-order approximation to the original energy in the time-discrete case. This is consistent with the modified energies from the IEQ or SAV approaches.

2.3. RRER method for the phase field crystal (PFC) model

Consider the free energy

$$E(\phi) = \int_{\Omega} \left(\frac{1}{2} \phi (a_0 + \Delta)^2 \phi + \frac{1}{4} \phi^4 - \frac{b_0}{2} \phi^2 \right) d\mathbf{x}, \tag{2.19}$$

and the mobility operator $\mathcal{G} = -\lambda \Delta$, where a_0, b_0 are two positive parameters such that $0 < b_0 < a_0$ and $b_0 \ll 1$, and $\lambda > 0$ is a parameter, and ϕ is a phase field variable which is introduced to describe the local atomic density field. Then the phase field model in (1.1) is specified as

$$\phi_t = \lambda \Delta \mu,$$

$$\mu = (a_0 + \Delta)^2 \phi + \phi^3 - b_0 \phi,$$
(2.20)

which is the so-called phase field crystal model (see [33-37]).

Introduce an auxiliary variable

$$q = \phi^2 - b_0 - \gamma,$$
 (2.21)

where $\gamma > 0$ is a stabilization parameter. Substituting (2.21) into (2.20), we have

$$\phi_t = \lambda \Delta \mu,$$

$$\mu = (a_0 + \Delta)^2 \phi + q \phi + \gamma \phi.$$

Then we obtain the following equivalent form of (2.20)

(a)
$$\phi_t = \lambda \Delta \mu$$
,
(b) $\mu = (a_0 + \Delta)g + q\phi + \gamma\phi$,
(c) $g = (a_0 + \Delta)\phi$,
(d) $q = \phi^2 - b_0 - \gamma$.

The modified energy can be obtained as follows

$$\hat{E}(\phi, q) = \frac{1}{2} \|\Delta\phi\|^2 - a_0 \|\nabla\phi\|^2 + \frac{1}{2} (\gamma + a_0^2) \|\phi\|^2 - \frac{1}{4} \|q\|^2 + \frac{1}{2} (q(\phi^2 - b_0 - \gamma), 1) - \frac{(\gamma + b_0)^2}{4} |\Omega|.$$
(2.23)

Remark 2.7. Similarly, we emphasize that the modified energy $\hat{E}(\phi, q)$ in (2.23) for the transformed model (2.22) is equivalent to the original energy $E(\phi)$ defined by (2.19). The derivation is shown below.

$$\begin{split} E(\phi) &= \int_{\Omega} \left(\frac{1}{2} \phi (a_0 + \Delta)^2 \phi + \frac{1}{4} \phi^4 - \frac{b_0}{2} \phi^2 \right) d\mathbf{x} \\ &= \int_{\Omega} \left(\frac{a_0^2}{2} \phi^2 + a_0 \phi \Delta \phi + \frac{1}{2} \phi \Delta^2 \phi + \frac{1}{4} (q + \gamma)^2 - \frac{b_0^2}{4} \right) d\mathbf{x} \\ &= \int_{\Omega} \left(\frac{a_0^2}{2} \phi^2 + a_0 \phi \Delta \phi + \frac{1}{2} \phi \Delta^2 \phi + \frac{1}{4} q^2 + \frac{\gamma}{2} ((\phi)^2 - b_0 - \gamma) + \frac{\gamma^2}{4} - \frac{b_0^2}{4} \right) d\mathbf{x} \\ &= \int_{\Omega} \left(\frac{1}{2} (a_0^2 + \gamma) \phi^2 + a_0 \phi \Delta \phi + \frac{1}{2} \phi \Delta^2 \phi + \frac{1}{4} q^2 - \frac{\gamma + b_0^2}{2} \right) d\mathbf{x} \\ &= \frac{1}{2} \|\Delta \phi\|^2 - a_0 \|\nabla \phi\|^2 + \frac{1}{2} (\gamma + a_0^2) \|\phi\|^2 - \frac{1}{4} \|q\|^2 + \frac{1}{2} (q(\phi^2 - b_0 - \gamma), 1) - \frac{(\gamma + b_0)^2}{4} |\Omega| \\ &= \hat{E}(\phi, q). \end{split}$$

Using the Crank-Nicolson scheme in time, we give a numerical approximation of (2.20) based on (2.22).

Algorithm 2. Assume that $(\phi^n, q^{n-\frac{1}{2}})$ are already calculated with $n \ge 1$. Then we compute the next step $(\phi^{n+1}, \mu^{n+\frac{1}{2}}, g^{n+\frac{1}{2}}, q^{n+\frac{1}{2}})$ from the following temporal discrete system:

(a)
$$\frac{\phi^{n+1} - \phi^n}{\delta t} = \lambda \Delta \mu^{n+\frac{1}{2}},$$
(b)
$$\mu^{n+\frac{1}{2}} = (a_0 + \Delta)g^{n+\frac{1}{2}} + q^{n+\frac{1}{2}} \frac{\phi^{n+1} + \phi^n}{2} + \gamma \frac{\phi^{n+1} + \phi^n}{2},$$
(c)
$$g^{n+\frac{1}{2}} = (a_0 + \Delta) \frac{\phi^{n+1} + \phi^n}{2},$$
(d)
$$\frac{q^{n+\frac{1}{2}} + q^{n-\frac{1}{2}}}{2} = (\phi^n)^2 - b_0 - \gamma.$$
(2.25)

Remark 2.8. Algorithm 2 is of second-order accuracy in time.

Remark 2.9. In practical implementation, we will use the following numerical approximation to compute $(\phi^1, q^{\frac{1}{2}})$

(a)
$$q^{\frac{1}{2}} = (\phi^0)^2 - b_0 - \gamma$$
,

(b)
$$\frac{\phi^1 - \phi^0}{\delta t} = \lambda \Delta \mu^{\frac{1}{2}},$$

(c)
$$\mu^{\frac{1}{2}} = (a_0 + \Delta)g^{\frac{1}{2}} + q^{\frac{1}{2}}\frac{\phi^1 + \phi^0}{2} + \gamma \frac{\phi^1 + \phi^0}{2}$$
,

(d)
$$g^{\frac{1}{2}} = (a_0 + \Delta) \frac{\phi^1 + \phi^0}{2}$$
.

Theorem 2.10. Algorithm 2 is unconditionally energy stable. Specifically, Algorithm 2 satisfies the following energy dissipation law: for any $n \ge 1$,

$$\hat{E}^{n+1}(\phi^{n+1}, q^{n+\frac{1}{2}}) - \hat{E}^{n}(\phi^{n}, q^{n-\frac{1}{2}}) = -\lambda \delta t \|\nabla \mu^{n+\frac{1}{2}}\|^{2} \le 0, \tag{2.26}$$

where the modified energy is defined as

$$\begin{split} \hat{E}^{n+1}(\phi^{n+1},q^{n+\frac{1}{2}}) = & \frac{1}{2} \|\Delta\phi^{n+1}\|^2 - a_0 \|\nabla\phi^{n+1}\|^2 + \frac{1}{2}(\gamma + a_0^2) \|\phi^{n+1}\|^2 \\ & - \frac{1}{4} \|q^{n+\frac{1}{2}}\|^2 + \frac{1}{2}(q^{n+\frac{1}{2}}[(\phi^{n+1})^2 - b_0 - \gamma], 1) - \frac{(\gamma + b_0)^2}{4} |\Omega|. \end{split}$$

Proof. Taking the inner product of (2.25)(a) with $\delta t \mu^{n+\frac{1}{2}}$, we get the equation

$$(\phi^{n+1} - \phi^n, (a_0 + \Delta)g^{n+\frac{1}{2}} + q^{n+\frac{1}{2}}\frac{\phi^{n+1} + \phi^n}{2} + \gamma\frac{\phi^{n+1} + \phi^n}{2}) = -\lambda\delta t \|\nabla \mu^{n+\frac{1}{2}}\|^2.$$

This can be reformulated as

J. Zhang, X. Guo, M. Jiang et al.

$$(\phi^{n+1} - \phi^n, (a_0 + \Delta)g^{n+\frac{1}{2}}) + \frac{1}{2}(q^{n+\frac{1}{2}}((\phi^{n+1})^2 - (\phi^n)^2), 1) + \frac{\gamma}{2}(\|\phi^{n+1}\|^2 - \|\phi^n\|^2) = -\lambda \delta t \|\nabla \mu^{n+\frac{1}{2}}\|^2.$$
(2.27)

We need to estimate the first two terms on the left-hand side of (2.27). Taking the inner product of (2.25)(c) with $a_0(\phi^{n+1} - \phi^n)$, we have

$$(a_0 g^{n+\frac{1}{2}}, \phi^{n+1} - \phi^n) = \frac{a_0^2}{2} (\|\phi^{n+1}\|^2 - \|\phi^n\|^2) - \frac{a_0}{2} (\|\nabla\phi^{n+1}\|^2 - \|\nabla\phi^n\|^2). \tag{2.28}$$

Meanwhile, taking the inner product of (2.25)(c) with $\Delta(\phi^{n+1} - \phi^n)$, we get

$$\begin{split} (g^{n+\frac{1}{2}}, \Delta(\phi^{n+1} - \phi^n)) = & (\Delta g^{n+\frac{1}{2}}, \phi^{n+1} - \phi^n) \\ = & \frac{a_0}{2} (\phi^{n+1} + \phi^n, \Delta(\phi^{n+1} - \phi^n)) + \frac{1}{2} (\|\Delta \phi^{n+1}\|^2 - \|\Delta \phi^n\|^2) \\ = & - \frac{a_0}{2} (\|\nabla \phi^{n+1}\|^2 - \|\nabla \phi^n\|^2) + \frac{1}{2} (\|\Delta \phi^{n+1}\|^2 - \|\Delta \phi^n\|^2). \end{split}$$

This can be simplified as

$$(\Delta g^{n+\frac{1}{2}}, \phi^{n+1} - \phi^n) = -\frac{a_0}{2} (\|\nabla \phi^{n+1}\|^2 - \|\nabla \phi^n\|^2) + \frac{1}{2} (\|\Delta \phi^{n+1}\|^2 - \|\Delta \phi^n\|^2). \tag{2.29}$$

Note that

$$q^{n+\frac{1}{2}}((\phi^{n+1})^2 - (\phi^n)^2) = q^{n+\frac{1}{2}}((\phi^{n+1})^2 - (\phi^n)^2) + q^{n-\frac{1}{2}}((\phi^n)^2 - (\phi^n)^2)$$

$$= q^{n+\frac{1}{2}}((\phi^{n+1})^2 - b_0 - \gamma) - q^{n-\frac{1}{2}}((\phi^n)^2 - b_0 - \gamma)$$

$$- (q^{n+\frac{1}{2}} - q^{n-\frac{1}{2}})((\phi^n)^2 - b_0 - \gamma).$$
(2.30)

Multiply (2.25)(d) by $q^{n+\frac{1}{2}} - q^{n-\frac{1}{2}}$, we have

$$(q^{n+\frac{1}{2}}-q^{n-\frac{1}{2}})((\phi^n)^2-b_0-\gamma)=\frac{1}{2}[(q^{n+\frac{1}{2}})^2-(q^{n-\frac{1}{2}})^2].$$

Substituting the above equation into (2.30), we have

$$q^{n+\frac{1}{2}}((\phi^{n+1})^2-(\phi^n)^2)=q^{n+\frac{1}{2}}((\phi^{n+1})^2-b_0-\gamma)-q^{n-\frac{1}{2}}((\phi^n)^2-b_0-\gamma)-\frac{1}{2}[(q^{n+\frac{1}{2}})^2-(q^{n-\frac{1}{2}})^2]. \tag{2.31}$$

Hence, for the second term on the left-hand side of (2.27), we note that

$$\begin{split} \frac{1}{2}(q^{n+\frac{1}{2}}((\phi^{n+1})^2-(\phi^n)^2),1) = &\frac{1}{2}(q^{n+\frac{1}{2}}((\phi^{n+1})^2-b_0-\gamma),1) - \frac{1}{2}(q^{n-\frac{1}{2}}((\phi^n)^2-b_0-\gamma),1) \\ &-\frac{1}{4}(\|q^{n+\frac{1}{2}}\|^2-\|q^{n-\frac{1}{2}}\|^2). \end{split} \tag{2.32}$$

Substituting the equations (2.28), (2.29) and (2.32) into (2.27), we get

$$\begin{split} &\frac{a_0^2}{2}\|\phi^{n+1}\|^2 - a_0\|\nabla\phi^{n+1}\|^2 + \frac{1}{2}\|\Delta\phi^{n+1}\|^2 + \frac{\gamma}{2}\|\phi^{n+1}\|^2 + \frac{1}{2}(q^{n+\frac{1}{2}}((\phi^{n+1})^2 - b_0 - \gamma), 1) - \frac{1}{4}\|q^{n+\frac{1}{2}}\|^2 \\ &- \frac{a_0^2}{2}\|\phi^n\|^2 + a_0\|\nabla\phi^n\|^2 - \frac{1}{2}\|\Delta\phi^n\|^2 - \frac{\gamma}{2}\|\phi^n\|^2 - \frac{1}{2}(q^{n-\frac{1}{2}}((\phi^n)^2 - b_0 - \gamma), 1) + \frac{1}{4}\|q^{n-\frac{1}{2}}\|^2 \\ &= -\lambda\delta t\|\nabla\mu^{n+\frac{1}{2}}\|^2. \end{split}$$

So we arrive at

$$\hat{E}^{n+1}(\phi^{n+1}, q^{n+\frac{1}{2}}) - \hat{E}^{n+1}(\phi^n, q^{n-\frac{1}{2}}) = -\lambda \delta t \|\nabla \mu^{n+\frac{1}{2}}\|^2 \le 0,$$

which indicates that our method is unconditionally energy-stable.

Remark 2.11. We briefly explore the connections between the modified energy and the original energy. Notice that

$$\begin{split} E(\phi^{n+1}) &\approx \hat{E}(\phi^{n+1},q^{n+1}) \\ &= \frac{1}{2} \|\Delta \phi^{n+1}\|^2 - a_0 \|\nabla \phi^{n+1}\|^2 + \frac{1}{2} (\gamma + a_0^2) \|\phi^{n+1}\|^2 \\ &- \frac{1}{4} \|q^{n+1}\|^2 + \frac{1}{2} (q^{n+1} [(\phi^{n+1})^2 - b_0 - \gamma], 1) - \frac{(\gamma + b_0)^2}{4} |\Omega| \\ &= \frac{1}{2} \|\Delta \phi^{n+1}\|^2 - a_0 \|\nabla \phi^{n+1}\|^2 + \frac{1}{2} (\gamma + a_0^2) \|\phi^{n+1}\|^2 \\ &- \frac{1}{4} \|q^{n+\frac{1}{2}}\|^2 + \frac{1}{2} (q^{n+\frac{1}{2}} [(\phi^{n+1})^2 - b_0 - \gamma], 1) - \frac{(\gamma + b_0)^2}{4} |\Omega| \\ &+ \frac{1}{2} (q^{n+1} [(\phi^{n+1})^2 - b_0 - \gamma], 1) - \frac{1}{2} (q^{n+\frac{1}{2}} [(\phi^{n+1})^2 - b_0 - \gamma], 1) - \frac{1}{4} \|q^{n+1}\|^2 + \frac{1}{4} \|q^{n+\frac{1}{2}}\|^2 \\ &= \hat{E}^{n+1} (\phi^{n+1}, q^{n+\frac{1}{2}}) + \frac{1}{2} (q^{n+1} [(\phi^{n+1})^2 - b_0 - \gamma], 1) \\ &- \frac{1}{2} (q^{n+\frac{1}{2}} [(\phi^{n+1})^2 - b_0 - \gamma], 1) - \frac{1}{4} \|q^{n+1}\|^2 + \frac{1}{4} \|q^{n+\frac{1}{2}}\|^2 \\ &\approx \hat{E}^{n+1} (\phi^{n+1}, q^{n+\frac{1}{2}}) + \frac{1}{4} (q^{n+1} - q^{n+\frac{1}{2}}, q^{n+1} - q^{n+\frac{1}{2}}). \end{split}$$

As we observe, the modified energy is a second-order approximation of the original energy in the time-discrete case.

Remark 2.12. Algorithm 2 also keeps mass conservation.

2.4. RRER method for coupled phase field equations

So far, the examples we have discussed contain a single phase variable and a single equation. We emphasize that our proposed relaxation technique applies to phase field models with multiple phase variables and coupled equations. Without loss of generality, we focus on the widely-used ternary phase field models (Cahn-Hilliard type coupled equations) and the multiphase models for grain growth (Allen-Cahn type coupled equations).

2.4.1. Ternary phase field model

The first example considers the ternary phase field model [39]. We use $\phi_i(\mathbf{x},t)$ to represent the volume fraction of phase i at location \mathbf{x} and time t. The total free energy for the ternary phase mixture can be postulated as

$$E(\phi_1, \phi_2, \phi_3) = \int_{\mathcal{L}} \left(\frac{3}{8} \sum_{i=1}^{3} \Sigma_i \varepsilon |\nabla \phi_i|^2 + \frac{12}{\varepsilon} F(\phi_1, \phi_2, \phi_3) \right) d\mathbf{x}, \tag{2.33}$$

where F is the bulk potential that is proposed as

$$F(\phi_1, \phi_2, \phi_3) = \sum_{i=1}^{3} \frac{\Sigma_i}{2} \phi_i^2 (1 - \phi_i)^2 + 3\Lambda \Pi_{i=1}^3 \phi_i^2.$$

Here Σ_i and Λ are parameters. We assume that the mixture is incompressible so that we have the constraint

$$\sum_{i=1}^{3} \phi_i(\mathbf{x}, t) = 0, \quad \forall (\mathbf{x}, t) \in \Omega \times [0, T].$$

$$(2.34)$$

Then, the ternary phase field model reads as

$$\begin{split} \partial_t \phi_i &= \frac{M_0}{\Sigma_i} \Delta \mu_i, \\ \mu_i &= -\frac{3}{4} \varepsilon \Sigma_i \Delta \phi_i + \frac{12}{\varepsilon} \frac{\partial F}{\partial \phi_i} + \beta_L, i = 1, 2, 3, \\ \beta_L &= -\frac{4\Sigma_T}{\varepsilon} \sum_{i=1}^3 \frac{1}{\Sigma_i} \frac{\partial F}{\partial \phi_i}, \\ \frac{\partial F}{\partial \phi_i} &= \Sigma_i \phi_i (1 - \phi_i) (1 - 2\phi_i) - \Sigma_i \gamma_i (1 - 2\phi_i) + 6 \Lambda \Pi_{j=1, j \neq i}^3 \phi_j^2 \phi_i, \end{split}$$

where Σ_T is chosen to satisfy $\frac{3}{\Sigma_T} = \frac{1}{\Sigma_1} + \frac{1}{\Sigma_2} + \frac{1}{\Sigma_3}$, and β_L is a Lagrangian multiplier to make sure the model satisfies the incompressibility condition in (2.34).

To design the relaxation numerical scheme, we introduce the auxiliary variables

$$q_i = \phi_i (1 - \phi_i) + \gamma_i, \quad s_i = \prod_{i=1}^3 \sum_{i \neq i} \phi_i^2, \quad i = 1, 2, 3,$$
 (2.35)

with $\gamma_i \ge 0$ the regularization parameters. With these auxiliary variables, the original ternary phase field model is reformulated as

$$\begin{split} & \partial_t \phi_i = \frac{M_0}{\Sigma_i} \Delta \mu_i, \\ & \mu_i = -\frac{3}{4} \varepsilon \Sigma_i \Delta \phi_i + \frac{12}{\varepsilon} \frac{\partial F}{\partial \phi_i} + \beta_L, i = 1, 2, 3, \\ & \beta_L = -\frac{4\Sigma_T}{\varepsilon} \sum_{i=1}^3 \frac{1}{\Sigma_i} \frac{\partial F}{\partial \phi_i}, \\ & \frac{\partial F}{\partial \phi_i} = \Sigma_i q_i (1 - 2\phi_i) - \Sigma_i \gamma_i (1 - 2\phi_i) + 6\Lambda s_i \phi_i, \\ & q_i = \phi_i (1 - \phi_i) + \gamma_i, i = 1, 2, 3, \\ & s_i = \Pi_{i=1}^3 \sum_{i \neq i} \phi_i^2, i = 1, 2, 3. \end{split}$$

Then, we can get the relaxation numerical scheme for the ternary phase field model.

Algorithm 3. Assume that $(\phi_i^n, q_i^{n-\frac{1}{2}}, s_i^{n-\frac{1}{2}})$, i = 1, 2, 3 are already calculated with $n \ge 1$. Then we compute the next step $(\phi_i^{n+1}, q_i^{n+\frac{1}{2}}, s_i^{n+\frac{1}{2}})$, i = 1, 2, 3 from the following temporal discrete system:

$$\frac{\phi_{i}^{n+1} - \phi_{i}^{n}}{\delta t} = \frac{M_{0}}{\Sigma_{i}} \Delta \mu_{i}^{n+\frac{1}{2}},
\mu_{i}^{n+\frac{1}{2}} = -\frac{3}{4} \varepsilon \Sigma_{i} \Delta \frac{\phi_{i}^{n+1} + \phi^{n}}{2} + \frac{12}{\varepsilon} \left[\frac{\partial F}{\partial \phi_{i}} \right]^{n+\frac{1}{2}} + \beta_{L}^{n+\frac{1}{2}}, i = 1, 2, 3,
\beta_{L}^{n+\frac{1}{2}} = -\frac{4\Sigma_{T}}{\varepsilon} \sum_{i=1}^{3} \frac{1}{\Sigma_{i}} \left[\frac{\partial F}{\partial \phi_{i}} \right]^{n+\frac{1}{2}},
\left[\frac{\partial F}{\partial \phi_{i}} \right]^{n+\frac{1}{2}} = \Sigma_{i} (q_{i}^{n+\frac{1}{2}} - \gamma_{i}) (1 - 2 \frac{\phi_{i}^{n+1} + \phi_{i}^{n}}{2}) + 6\Lambda s_{i}^{n+\frac{1}{2}} \frac{\phi_{i}^{n+1} + \phi_{i}^{n}}{2},
\frac{q_{i}^{n+\frac{1}{2}} + q_{i}^{n-\frac{1}{2}}}{2} = \phi_{i}^{n} (1 - \phi_{i}^{n}) + \gamma_{i}, i = 1, 2, 3,
\frac{s_{i}^{n+\frac{1}{2}} + s_{i}^{n-\frac{1}{2}}}{2} = \Pi_{j=1, j \neq i}^{3} (\phi_{j}^{2})^{n}, i = 1, 2, 3.$$
(2.36)

The Algorithm 3 is linear and second-order accurate in time. γ_i acts as a regularization parameter. q_i and s_i are the intermediate variables to linearize the scheme since they are discretized in staggered time meshes.

2.4.2. Phase field model for grain growth

In the second example, we consider the phase field model for grain growth that was introduced in [38]. Consider a mixture of m phases. Define the free energy

$$E = \int_{\Omega} \left[\sum_{i=1}^{m} \frac{\kappa_i}{2} |\nabla \phi_i|^2 + F(\phi_1, \phi_2, \dots, \phi_m) \right] d\mathbf{x},$$

with κ_i the gradient energy coefficients, and F the bulk free energy density. The main requirement for F is that it has m degenerate minima with equal depth, located as $(\phi_1, \phi_2, \dots, \phi_m) = (1, 0, \dots, 0), (0, 1, \dots, 0), \dots, (0, 0, \dots, 1)$ in m dimension space. One particular case for F could be

$$F = \sum_{i=1}^{m} (-\frac{\alpha}{2}\phi_i^2 + \frac{\beta}{4}\phi_i^4) + \gamma \sum_{i=1}^{m} \sum_{j=1}^{m} \phi_i^2 \phi_j^2,$$

with α , β and γ are the model parameters. The dynamics is governed by the Ginzburg-Landau equation

$$\partial_t \phi_i = -L_i \frac{\delta E}{\delta \phi_i}, \quad i = 1, 2, \cdots, m,$$

with L_i some positive constants. It can be expanded as

$$\partial_t \phi_i = -L_i \left(-\kappa_i \Delta \phi_i - \alpha \phi_i + \beta \phi_i^3 + 2\gamma \phi_i \sum_{i \neq i}^m \phi_j^2 \right), \quad i = 1, 2, \cdots, m.$$
 (2.37)

To derive the relaxation numerical scheme, we can introduce

$$q_i = \phi_i^2 - \gamma_i, \quad s_i = \sum_{i \neq i}^m \phi_j^2, \quad i = 1, 2, \dots, m,$$
 (2.38)

with γ_i the regularization parameters. We can rewrite the grain growth model in (2.37) as

$$\begin{split} \partial_t \phi_i &= -L_i \Big(-\kappa_i \Delta \phi_i - \alpha \phi_i + \beta (q_i + \gamma_i) \phi_i + 2\gamma \phi_i s_i \Big), i = 1, 2, \cdots, m, \\ q_i &= \phi_i^2 - \gamma_i, \quad i = 1, 2, \cdots, m, \\ s_i &= \sum_{i \neq i}^m \phi_j^2, \quad i = 1, 2, \cdots, m. \end{split}$$

We use the second-order Crank-Nicolson method to discretize the above model for temporal discretization. With this method, we can obtain the following discrete scheme.

Algorithm 4. Assume that $(\phi_i^n, q_i^{n-\frac{1}{2}}, s_i^{n-\frac{1}{2}})$ are already calculated with $n \ge 1$. Then we compute the next step $(\phi_i^{n+1}, q_i^{n+\frac{1}{2}}, s_i^{n+\frac{1}{2}})$ from the following temporal discrete system:

$$\begin{split} \frac{\phi_{i}^{n+1}-\phi_{i}^{n}}{\delta t} &= -L_{i}\bigg((-\kappa_{i}\Delta-\alpha+\beta q_{i}^{n+\frac{1}{2}}+\beta\gamma_{i}+2\gamma s_{i}^{n+\frac{1}{2}})\frac{\phi_{i}^{n+1}+\phi_{i}^{n}}{2}\bigg), \quad i=1,2,\cdots,m, \\ \frac{q_{i}^{n+\frac{1}{2}}+q_{i}^{n-\frac{1}{2}}}{2} &= (\phi_{i}^{n})^{2}-\gamma_{i}, \quad i=1,2,\cdots,m, \\ \frac{s_{i}^{n+\frac{1}{2}}+s_{i}^{n-\frac{1}{2}}}{2} &= \sum_{i\neq i}^{m}\phi_{j}^{2}, \quad i=1,2,\cdots,m. \end{split}$$

Similarly, Algorithm 4 is linear and second-order accurate in time. A mesh refinement test is further provided to justify the second-order temporal convergence in the next section.

3. Numerical experiments

This section presents some numerical examples to confirm our theoretical analysis. For simplicity, we consider only the periodic boundary condition and use the standard finite element method for spatial discretization. And the algorithms are implemented using FreeFEM [41]. The details for spatial discretization are omitted.

3.1. Convergence rate test

Throughout this subsection, we set $\gamma=2.0$ for convenience. The computational domain is $\Omega=[0,1]\times[0,1]$, the time interval is [0,T]=[0,1], and we use the spatial mesh size h. To test the convergence rate of our proposed methods, we take the exact solution as $\phi(x,y,t)=e^{-t}\cos(\pi x)\cos(\pi y)$ for both the MBE model and the PFC model. The corresponding right-hand side terms can be computed using the exact solution. Additionally, we set $\epsilon=1$ for the MBE model, while we use $a_0=1.0$, $b_0=0.01$, and $\lambda=1.0$ for the PFC model.

In practical implementation, we take $\delta t = h$ and use the P1 finite element space for both models. For different mesh sizes h, we present numerical results obtained using the RRER, IEQ, and exponential SAV (ESAV) algorithms in Table 1 and Table 2. These numerical results show that the RRER algorithm demonstrates second-order convergence in both space and time, similar to IEQ and ESAV algorithms. Notably, for the PFC model, our proposed RRER algorithm produces more accurate numerical results than IEQ and ESAV algorithms.

Furthermore, we also compare the computational efficiency of the IEQ, ESAV, and RRER methods. The computational time is provided in Table 3. It is evident that the RRER method takes less time than other methods, indicating that our method can improve computational efficiency.

We also implemented the scheme in (2.39). Consider the domain $\Omega = [0,1] \times [0,1]$. The model parameters of the coupled system in (2.37) are chosen as follows:

$$m = 3$$
, $L_1 = L_2 = L_3 = 1$, $\alpha = \beta = \gamma = 1$, $k_1 = k_2 = k_3 = 2$.

Table 1
Numerical results for MBE by RRER, IEQ, and ESAV algorithms.

δt	RRER		IEQ		ESAV	
	Errors	Rates	Errors	Rates	Errors	Rates
1 0	3.2923e-03	-	3.0372e-03	-	3.2923e-03	-
8 1 16	8.2307e-04	2.00	7.9218e-04	1.94	8.2307e-04	2.00
10 10 32	2.0577e-04	2.00	2.0197e-04	1.97	2.0577e-04	2.00
16 1 32 1 64 1	5.1442e-05	2.00	5.0971e-05	1.99	5.1442e-05	2.00
128	1.2861e-05	2.00	1.2802e-05	1.99	1.2861e-05	2.00

Table 2Numerical results for PFC by RRER, IEQ, and ESAV algorithms.

δt	RRER		IEQ		ESAV	
	Errors	Rates	Errors	Rates	Errors	Rates
1 8 1	3.2923e-03	-	3.2923e-03	-	3.4785e-03	-
	8.2307e-04	2.00	1.1259e-03	1.55	1.1557e-03	1.59
16 1 32	2.0577e-04	2.00	3.0931e-04	1.86	3.1249e-04	1.89
	5.1442e-05	2.00	7.9890e-05	1.95	8.02011e-05	1.96
$\frac{64}{1}$	1.2861e-05	2.00	2.0208e-05	1.98	2.02375e-05	1.99

Table 3Comparison of computational time.

model	RRER	IEQ	ESAV
MBE	103.76	207.18	222.22
PFC	552.45	949.37	656.49

Table 4Convergence test results for the grain growth model.

h	Convergence rates in time						
	L^2 for ϕ_1	rate	L^2 for ϕ_2	rate	L^2 for ϕ_3	rate	
1/8	7.25e-01	-	9.30e-02	-	6.60e-02	-	
1/16	2.11e-01	1.8	3.10e-02	1.6	3.03e-02	1.1	
1/32	5.33e-02	2.0	7.93e-03	2.0	7.94e-03	2.0	
1/64	1.33e-02	2.0	1.98e-03	2.0	1.99e-03	2.0	
1/128	3.33e-03	2.0	4.96e-04	2.0	4.98e-04	2.0	
1/256	8.33e-04	2.0	1.24e-04	2.0	1.25e-04	2.0	

We set the exact solution as:

$$\begin{cases} \phi_1 = 0.3\cos(\pi x)\cos(\pi y)e^{-t}, \\ \phi_2 = 0.1\cos(5\pi x)\cos(5\pi y)e^{-2t}, \\ \phi_3 = 0.1\cos(3\pi x)\cos(3\pi y)e^{-3t}, \end{cases}$$

and chose the regularization parameters $\gamma_1 = \gamma_2 = \gamma_3 = 2$. In practical implementation, we take $\delta t = h$ and use the P1 finite element space for both models. As shown in Table 4, a second-order accuracy is observed for all variables.

3.2. Numerical tests for energy dissipation and mass conservation

Here, we will test the energy dissipation and mass conservation properties. The initial condition is $\phi(x, y, 0) = \cos \pi x \cos \pi y$, and the other model parameters are chosen as in the above subsection. For different time steps δt and the interface width parameter ϵ , we present the original and modified numerical energies in Fig. 1 for the MBE and PFC models. These numerical results suggest that our methods are unconditionally energy-stable. Additionally, we provide numerical mass results in Fig. 2 for the MBE and PFC models with $\delta t = 0.1$. These results demonstrate that our methods are mass conservative.

3.3. Numerical examples of the MBE model in 2D

We set the domain $\Omega = [0, 2\pi] \times [0, 2\pi]$, and the parameters $\epsilon^2 = 0.1$ and $\gamma = 20$. The initial condition is chosen as $\phi(x, y, 0) = 0.1(\sin 3x \sin 2y + \sin 5x \sin 5y)$. Using a mesh size $h = 2\pi/128$ and time step $\delta t = 10^{-4}$, the MBE model is solved using Algorithm 1.

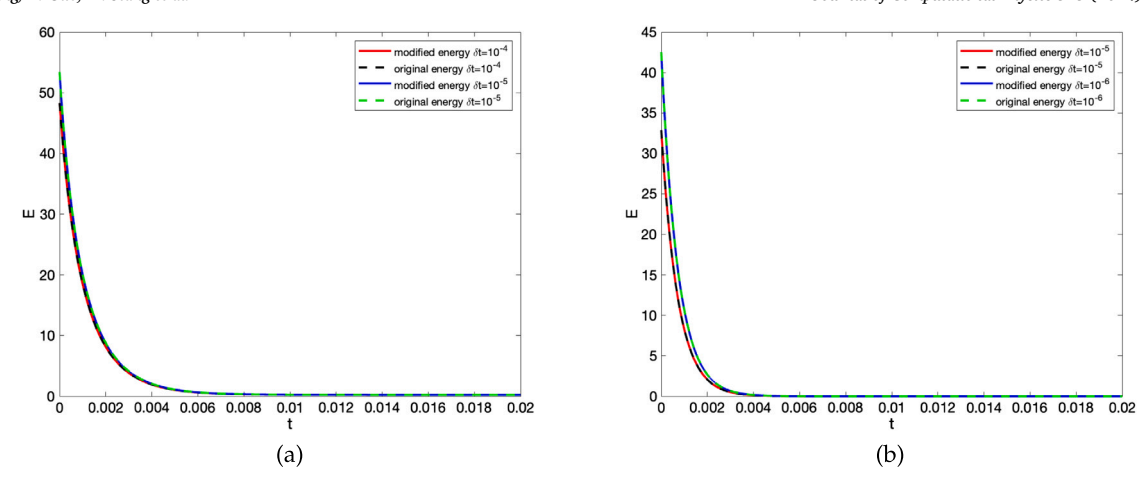


Fig. 1. Numerical energy results for the MBE and PFC model with a different time step δt : (a) MBE, (b) PFC.

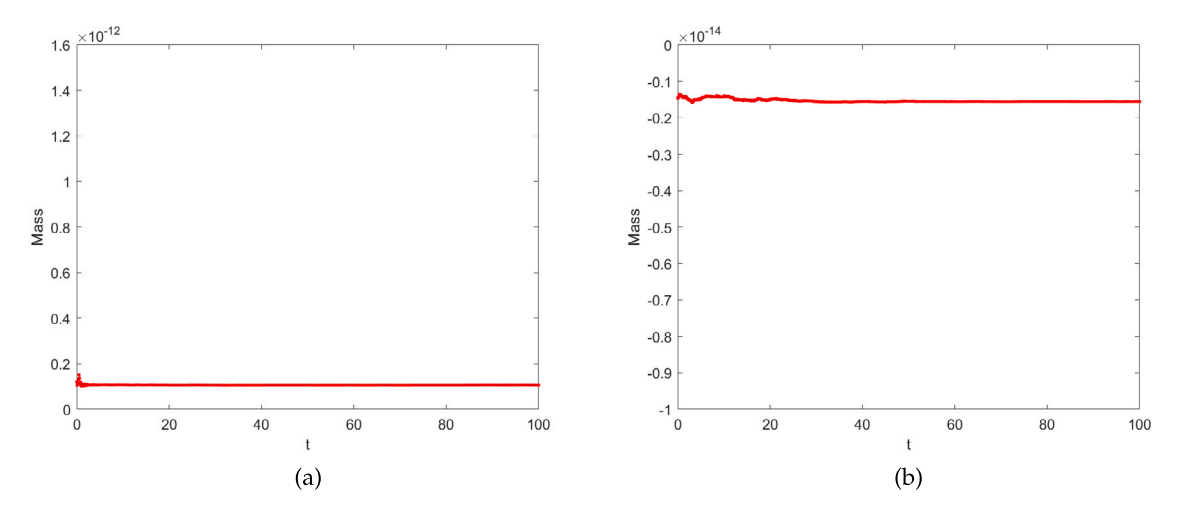


Fig. 2. Numerical mass results for both MBE model (a) $\gamma=20$, $\epsilon=1.0$ and PFC model (b) $\gamma=1.0$, $a_0=1.0$, $b_0=0.325$, $\delta t=0.1$.

We present the contour lines of the numerical solutions of ϕ up to the steady state. As shown in Fig. 3, our numerical results are consistent with the phase diagram of the MBE model with slope selection as reported in [29].

3.4. Numerical examples of the PFC model in 2D

Furthermore, we conduct several numerical tests using Algorithm 2 to solve the PFC model. We firstly consider the two-dimensional example on $\Omega = [0,100] \times [0,100]$. The initial condition is chosen as $\phi(x,y,0) = \hat{\phi}_0 + 0.01 rand(x,y)$, where $\hat{\phi}_0$ is a constant and rand(x,y) generates random numbers between -1 and 1. We set the parameters as $a_0 = 1.0$, $b_0 = 0.35$, T = 200 and $\gamma = 2.0$. The spatial mesh size is h = 100/128, and the time step is $\delta t = 0.1$. For different values of $\hat{\phi}_0$, the numerical results are summarized with P1-element in Fig. 4 and Fig. 5. A stripe pattern is observed with $\hat{\phi}_0 = 0$ as shown in Fig. 4, and a triangle pattern is observed with $\hat{\phi}_0 = 0.2$ as shown in Fig. 5. These results are consistent with the phase diagram of the PFC model as reported in the literature [33].

3.5. Numerical examples of the PFC model on curved surfaces

We first study the PFC model on a spherical surface with a radius of R = 64. We use a random initial condition, and the parameters are chosen as in the 2D case. For different values of $\hat{\phi}_0$, we summarize snapshots of the numerical approximation for ϕ at times t = 50, t = 100, t = 200 with $\delta t = 0.1$, Depending on the value of $\hat{\phi}_0$, we observe different patterns, such as striped as shown in Fig. 6 and hexagonal as shown in Fig. 7. These numerical results are consistent with the reported results in [36].

Next, we consider the ring torus domain with an outer radius of R = 50 and an inner radius of r = 20. We set the mesh size to h = 1 and the time increment to $\delta t = 0.1$. The other parameters are chosen as previously described. Snapshots of the numerical approximation of ϕ with different initial values $\hat{\phi}_0$ are plotted at times t = 50, 100, and 200 in Fig. 8 and Fig. 9. As expected,

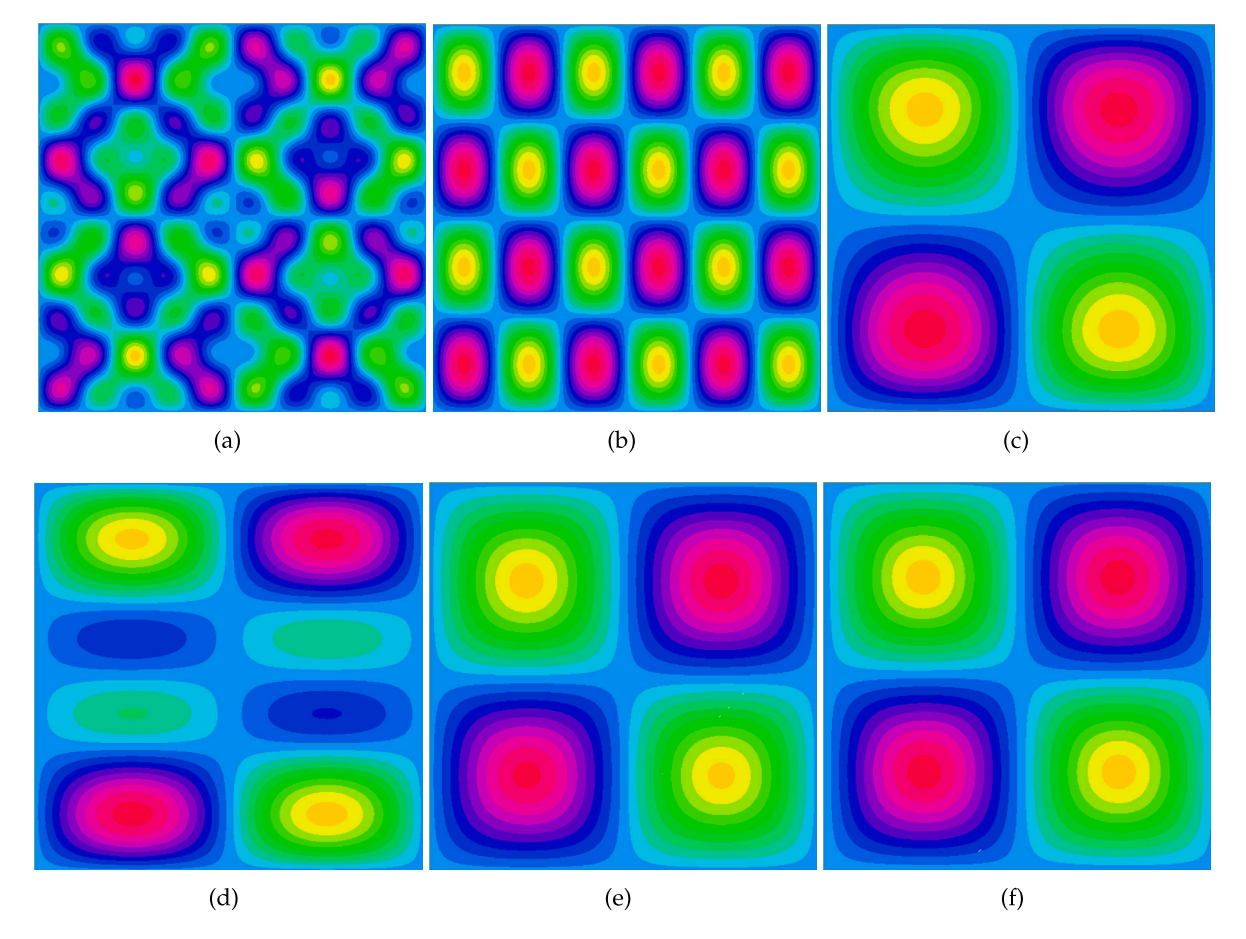


Fig. 3. The Snapshots of numerical solutions of the function ϕ at time (a) t = 0, (b) t = 0.05, (c) t = 2.5, (d) t = 8, (e) t = 15, (f) t = 30.

depending on the different initial values of ϕ , we observe stripe pattern formation as shown in Fig. 8 and hexagonal pattern formation as shown in Fig. 9.

Meanwhile, we also consider the cube surface case. The computational domain is $\Omega = [0, 100] \times [0, 100] \times [0, 100]$. We start with a random initial condition. The parameters a_0 , b_0 , and γ are the same as in the 2D case. For this case, we present snapshots of the numerical approximation of ϕ with h = 100/64 and $\delta t = 0.1$ in Fig. 10 and Fig. 11. These results show similar dynamics as those in [36].

3.6. Numerical examples of the PFC model in 3D

Finally, we simulate the phase separation dynamics in 3D by solving the PFC model with our proposed numerical algorithm. The computational domain is $\Omega = [0,128] \times [0,128] \times [0,128]$. We start with a random initial condition, and employ the same model parameters a_0 , b_0 , and γ as in the 2D case. The space mesh is set to h=2 and the time step $\delta t=10^{-2}$. Numerical snapshots of ϕ at different times with various $\hat{\phi}_0$ values are presented in Fig. 12 and Fig. 13. These results exhibit similar dynamics to those reported in [35].

4. Conclusion

In this paper, we construct the linear relaxation with regularized energy reformulation approaches for phase field models. In these approaches, we avoid taking the time derivative of the auxiliary variables by discretizing them on a staggered time mesh. Consequently, we only need to solve an algebraic equation for the introduced auxiliary variables and then bring them into the equivalent equations. We rigorously establish the unconditional energy-stable properties of the proposed schemes for the MBE and PFC models. A series of numerical examples are provided to test the accuracy of the proposed schemes and demonstrate the efficiency in simulating the dynamics driven by the MBE and PFC models. Additionally, we anticipate that the time-fractional phase field models, such as time-fractional Allen-Cahn and Cahn-Hilliard phase-field models (see [7,8,13,26]), can also be studied within our framework, which will be our focus in the near future.

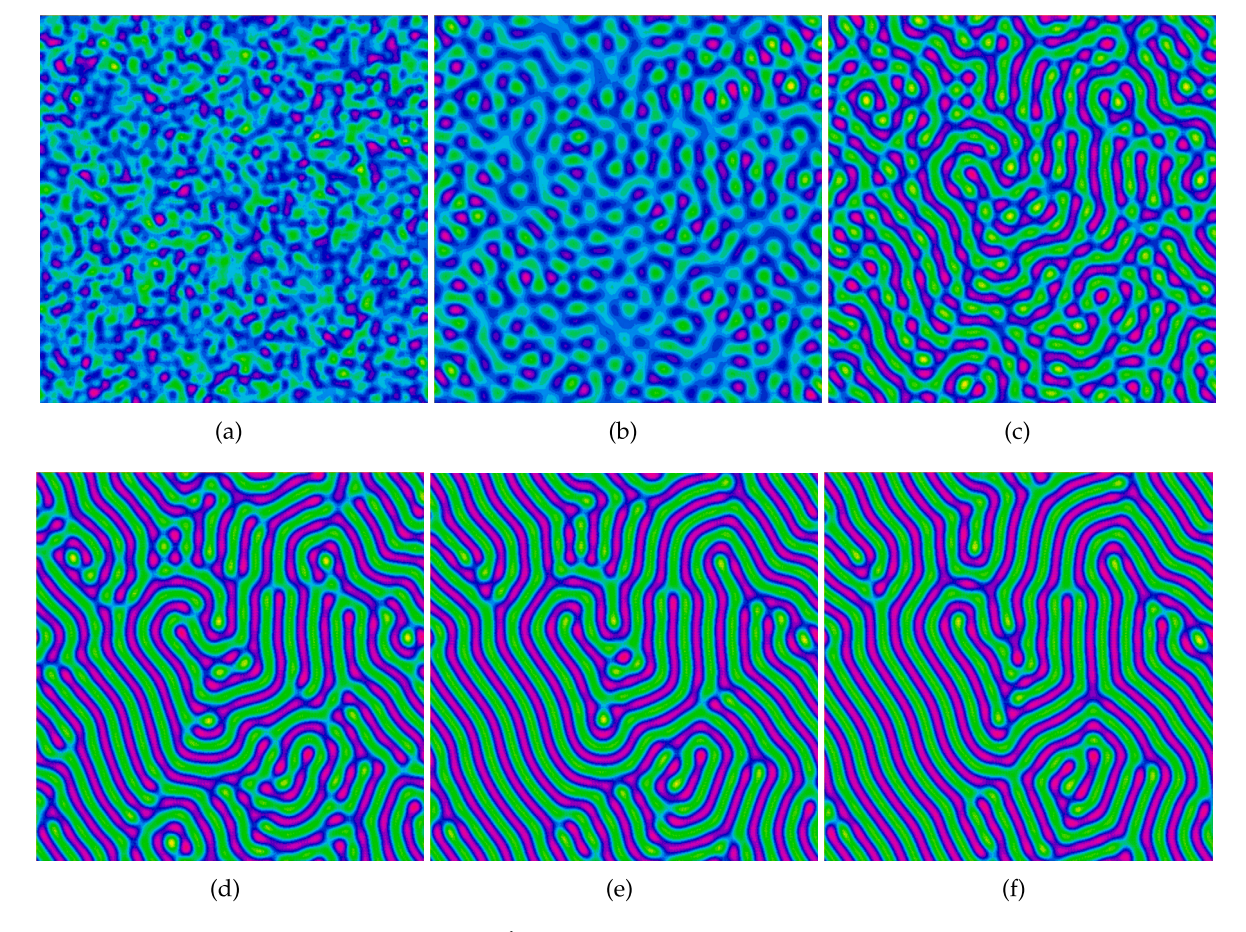


Fig. 4. Crystal growth pattern formation with $\hat{\phi}_0 = 0$ at time (a) t = 1, (b) t = 15, (c) t = 30, (d) t = 50, (e) t = 100, (f) t = 200.

CRediT authorship contribution statement

Jiansong Zhang: Conceptualization, Formal analysis, Methodology, Validation, Writing – original draft, Writing – review & editing. Xinxin Guo: Conceptualization, Formal analysis, Validation, Writing – original draft, Writing – review & editing, Methodology. Maosheng Jiang: Conceptualization, Formal analysis, Investigation, Validation, Writing – review & editing, Methodology. Tao Zhou: Conceptualization, Methodology, Writing – review & editing. Jia Zhao: Conceptualization, Methodology, Supervision, Writing – review & editing.

Declaration of competing interest

The authors declare that they have no known competing financial interests or personal relationships that could have appeared to influence the work reported in this paper.

Data availability

No data was used for the research described in the article.

Acknowledgements

J. Zhang's work was supported by the Natural Science Foundation of Shandong Province (No. ZR2023MA081) and the Fundamental Research Funds for the Central Universities (No. 22CX03020A). M. Jiang's work was partially supported by the National Natural Science Foundation of China (No. 12071046), the Natural Science Foundation of Shandong Province (No. ZR2021QA018) and China Postdoctoral Science Foundation Funded Projection (No. 2022M721757). T. Zhou's work was supported by NSF of China (No. 12288201), the youth innovation promotion association (CAS), and Henan Academy of Sciences. J. Zhao would like to acknowledge the support from the USA's National Science Foundation (NSF) with grant DMS-2111479/2405605.

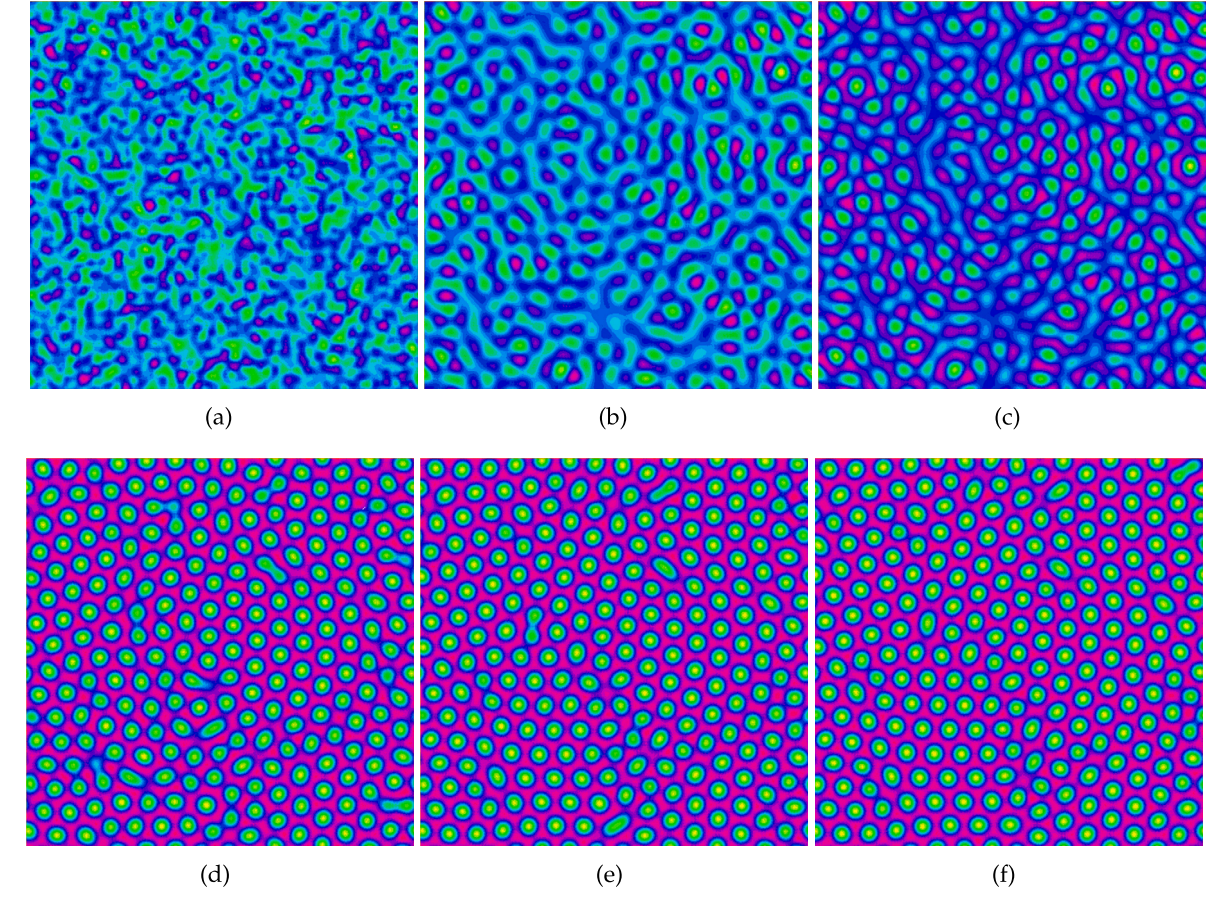


Fig. 5. Crystal growth pattern formation with $\hat{\phi}_0 = 0.2$ at time (a) t = 1, (b) t = 15, (c) t = 30, (d) t = 50, (e) t = 100, (f) t = 200.

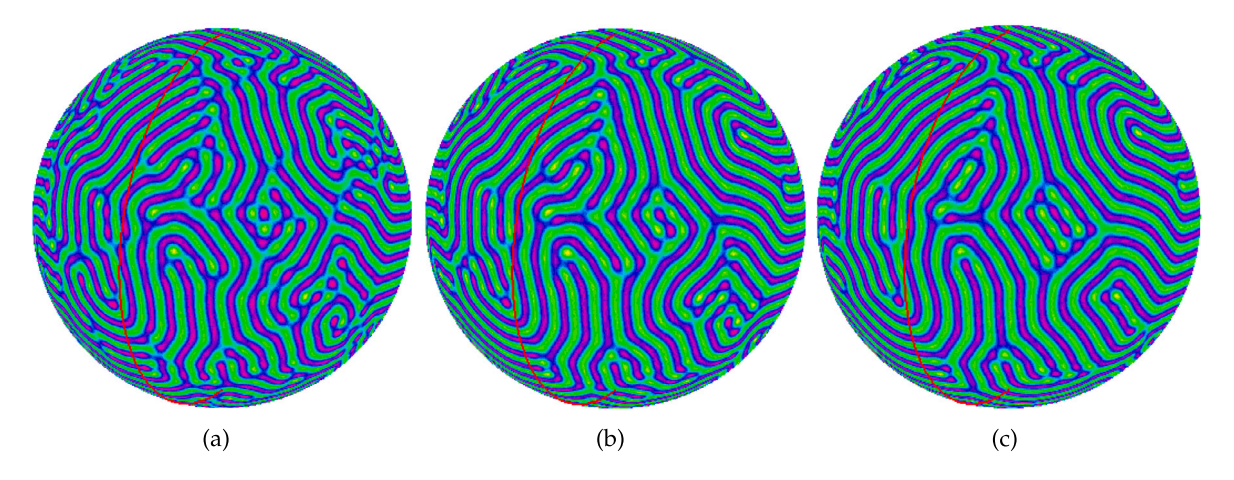


Fig. 6. PFC dynamics on a spherical surface with $\hat{\phi}_0 = 0$ at time (a) t = 50, (b) t = 100, (c) t = 200.

References

- [1] Ingo Steinbach, Phase-field models in materials science, Model. Simul. Mater. Sci. Eng. 17 (2009) 073001.
- [2] Long-Qing Chen, Phase-field models for microstructure evolution, Annu. Rev. Mater. Res. 32 (2002) 113–140.
- [3] J. Cahn, J. Hilliard, Free energy of a nonuniform system. I. Interfacial free energy, J. Chem. Phys. 28 (1958) 258–267.
- [4] Y. Gong, J. Zhao, Q. Wang, Linear second order in time energy stable schemes for hydrodynamic models of binary mixtures based on a spatially pseudospectral approximation, Adv. Comput. Math. 44 (2018) 1573–1600.
- [5] X. Li, V. Cristini, Q. Nie, J. Lowengrub, Nonlinear three-dimensional simulation of solid tumor growth, Discrete Contin. Dyn. Syst., Ser. B 7 (2007) 581-604.

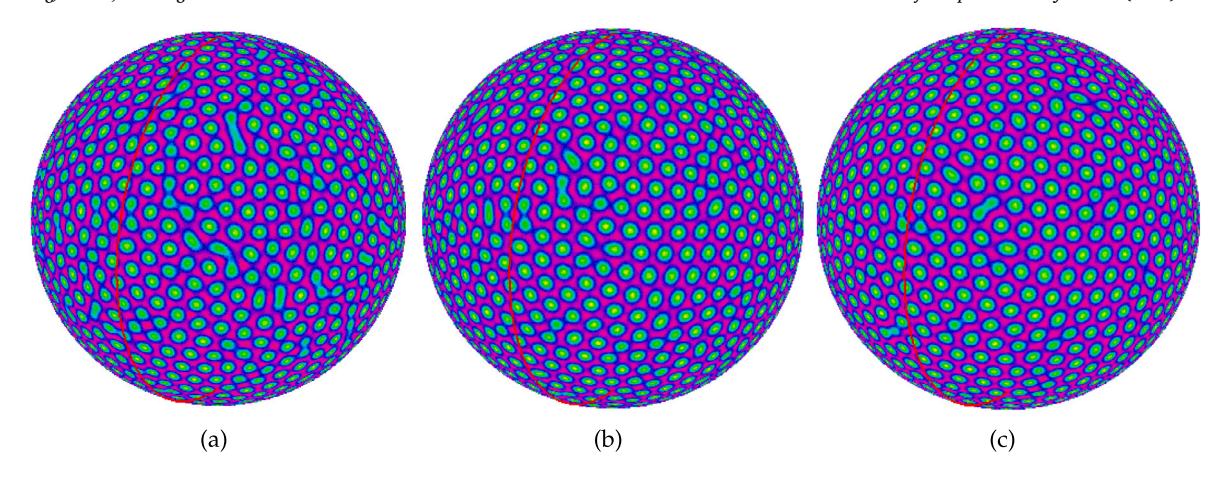


Fig. 7. PFC dynamics on a spherical surface with $\hat{\phi}_0 = 0.2$ at time (a) t = 50, (b) t = 100, (c) t = 200.

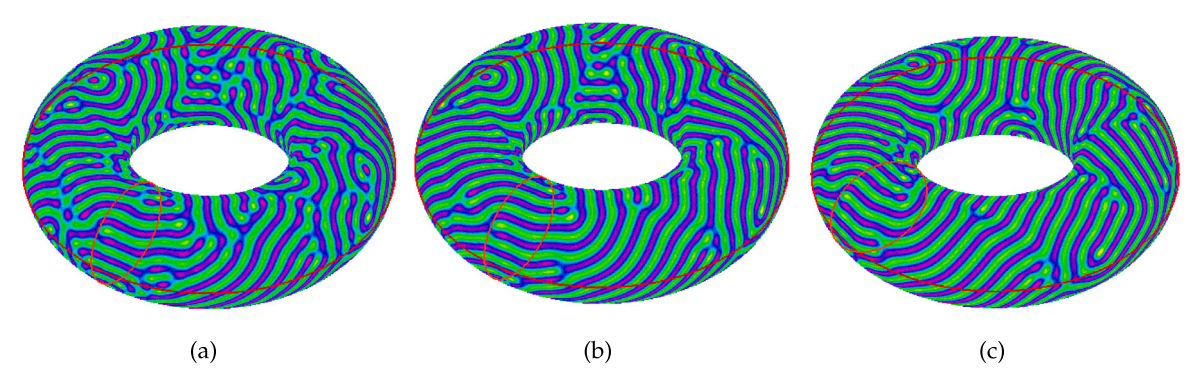


Fig. 8. PFC dynamics on a toroidal surface with $\hat{\phi}_0 = 0$ at time (a) t = 50, (b) t = 100, (c) t = 200.

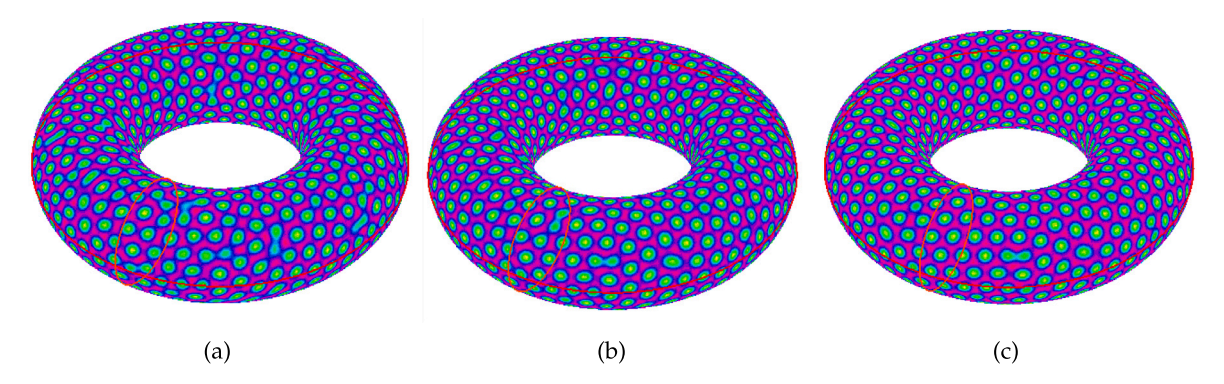


Fig. 9. PFC dynamics on a toroidal surface with $\hat{\phi}_0 = 0.2$ at time (a) t = 50, (b) t = 100, (c) t = 200.

- [6] X. Xu, Y. Di, H. Yu, Sharp-interface limits of a phase-field model with a generalized Navier slip boundary condition for moving contact lines, J. Fluid Mech. 849 (2018) 805–833.
- [7] T. Tang, H. Yu, T. Zhou, On energy dissipation theory and numerical stability for time-fractional phase-field equations, SIAM J. Sci. Comput. 41 (2019) A3757–A3778.
- [8] H. Liao, T. Tang, T. Zhou, A second-order and nonuniform time-stepping maximum-principle preserving scheme for time-fractional Allen-Cahn equations, J. Comput. Phys. 414 (2020) 109473.
- [9] W.B. Chen, J.Y. Jing, C. Wang, X.M. Wang, S.M. Wise, A modified Crank-Nicolson numerical scheme for the Flory-Huggins Cahn-Hilliard model, Commun. Comput. Phys. 31 (2022) 60–93.
- [10] J. Shen, C. Wang, X. Wang, S.M. Wise, Second-order convex splitting schemes for gradient flows with Ehrlich- Schwoebel type energy: application to thin film epitaxy, SIAM J. Numer. Anal. 50 (2012) 105–125.
- [11] J. Shin, H.G. Lee, J.-Y. Lee, First and second order numerical methods based on a new convex splitting for phase-field crystal equation, J. Comput. Phys. 327 (2016) 519–542.
- [12] J. Shin, H.G. Lee, J.-Y. Lee, Convex splitting Runge-Kutta methods for phase-field models, Comput. Math. Appl. 73 (11) (2017) 2388-2403.
- [13] Q. Du, J. Yang, Z. Zhou, Time-fractional Allen-Cahn equations: analysis and numerical methods, J. Sci. Comput. 85 (2020) 2.

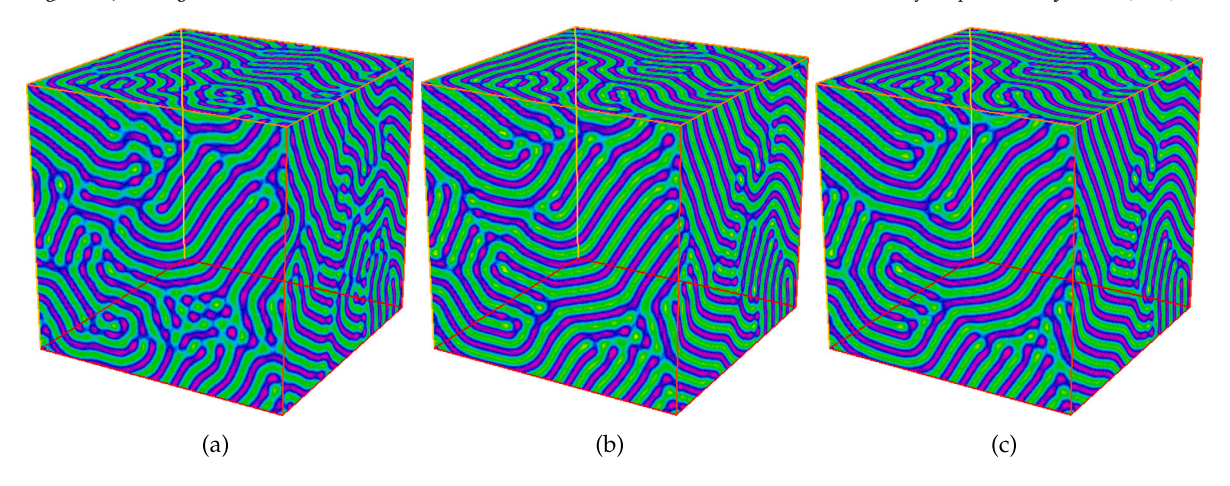


Fig. 10. Stripe pattern formation with $\hat{\phi}_0 = 0$ at time (a) t = 50, (b) t = 100, (c) t = 200.

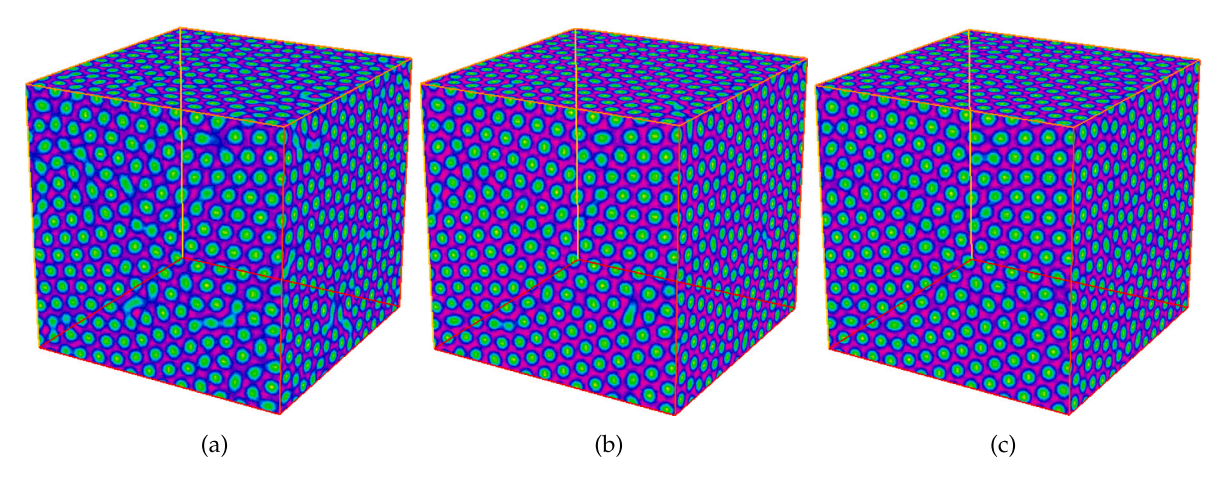


Fig. 11. Hexagonal pattern formation with $\hat{\phi}_0 = 0.2$ at time (a) t = 50, (b) t = 100, (c) t = 200.

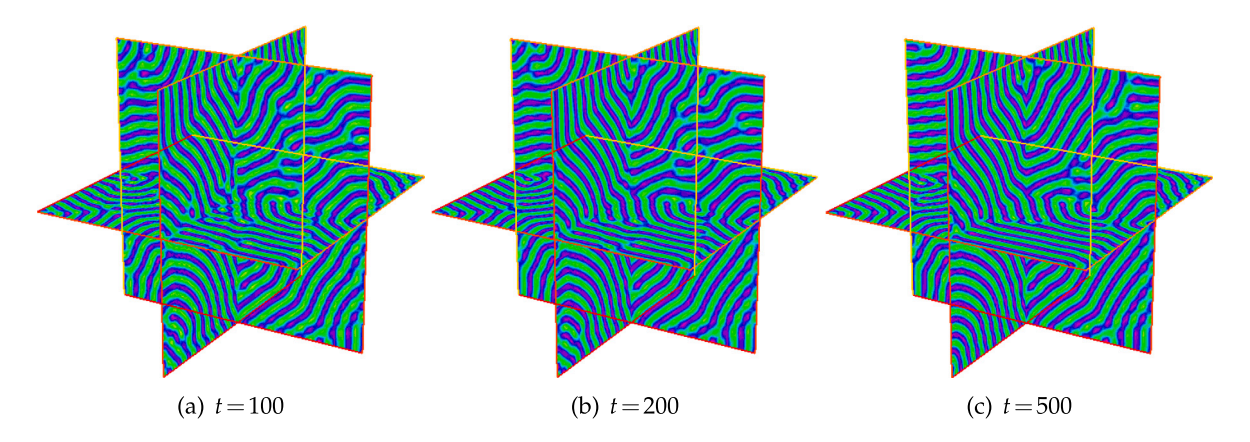


Fig. 12. Stripe pattern formation with $\hat{\phi}_0 = 0$ at different times. The 3-slice views are provided for a better visualization of the 3D dynamics.

- [14] Q. Du, L. Ju, X. Li, Z. Qiao, Maximum bound principles for a class of semilinear parabolic equations and exponential time-differencing schemes, SIAM Rev. 63 (2021) 317–359.
- [15] L. Ju, Q. Du, Z. Qiao, Maximum principle preserving exponential time differencing schemes for the nonlocal Allen–Cahn equation, SIAM J. Numer. Anal. 57 (2019) 875–898.
- [16] X. Wang, L. Ju, Q. Du, Efficient and stable exponential time differencing Runge-Kutta methods for phase field elastic bending energy models, J. Comput. Phys. 316 (2016) 21–38.
- [17] Y. Gong, J. Zhao, Q. Wang, Arbitrarily high-order unconditionally energy stable schemes for thermodynamically consistent gradient flow models, SIAM J. Sci. Comput. 42 (2020) B135–B156.

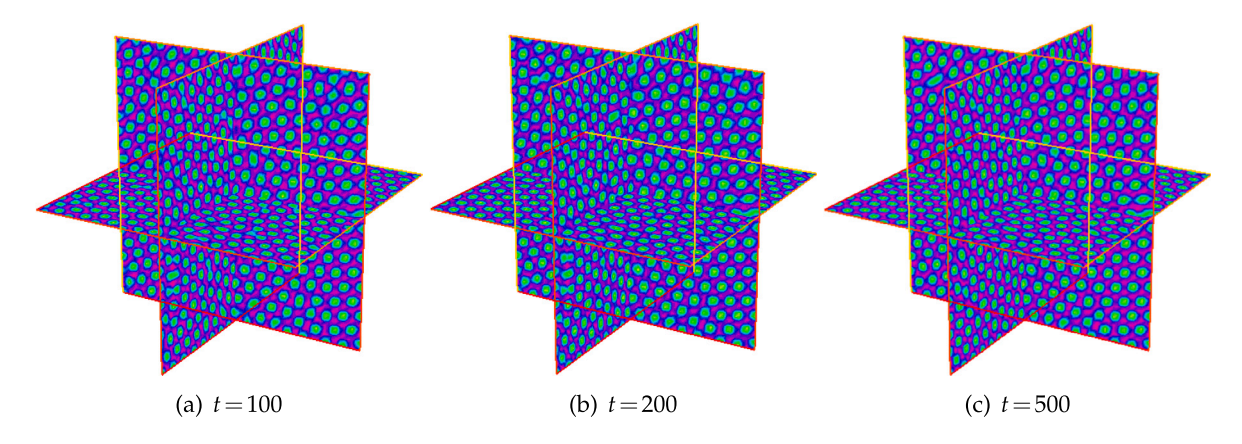


Fig. 13. Triangle pattern formation with $\hat{\phi}_0 = 0.2$ at different times. The 3-slice views are provided for a better visualization of the 3D dynamics.

- [18] X. Yang, Linear, first and second-order, unconditionally energy stable numerical schemes for the phase field model of homopolymer blends, J. Comput. Phys. 327 (2016) 294–316.
- [19] X. Yang, H. Yu, Efficient second order unconditionally stable schemes for a phase field moving contact line model using an invariant energy quadratization approach, SIAM J. Sci. Comput. 40 (2018) B889–B914.
- [20] J. Zhao, A revisit of the energy quadratization method with a relaxation technique, Appl. Math. Lett. 120 (2021) 107331.
- [21] X. Yang, Efficient and energy stable scheme for the hydrodynamically coupled three components Cahn-Hilliard phase-field model using the stabilized-invariant energy quadratization (S-IEQ) approach, J. Comput. Phys. 438 (2021) 110342.
- [22] J. Shen, J. Xu, J. Yang, The scalar auxiliary variable (SAV) approach for gradient flows, J. Comput. Phys. 353 (2018) 407-416.
- [23] J. Shen, J. Xu, J. Yang, A new class of efficient and robust energy stable schemes for gradient flows, SIAM Rev. 61 (2019) 474-506.
- [24] F. Huang, J. Shen, Z. Yang, A highly efficient and accurate new scalar auxiliary variable approach for gradient flows, SIAM J. Sci. Comput. 42 (2020) A2514–A2536.
- [25] J. Shen, J.X. Li, H. Rui, Energy stability and convergence of SAV block-centered finite difference method for gradient flows, Math. Comput. 88 (2019) 2047–2068.
- [26] Y. Yu, J. Zhang, R. Qin, The exponential SAV approach for the time-fractional Allen-Cahn and Cahn-Hilliard phase-field models, J. Sci. Comput. 94 (2023) 33.
- [27] Q. Cheng, C. Liu, J. Shen, A new Lagrange multiplier approach for gradient flows, Comput. Methods Appl. Mech. Eng. 367 (2020) 113070.
- [28] J. Shen, X. Yang, Numerical approximations of Allen-Cahn and Cahn-Hilliard equations, Discrete Contin. Dyn. Syst. 28 (2010) 1669-1691.
- [29] L. Chen, J. Zhao, X. Yang, Regularized linear schemes for the molecular beam epitaxy model with slope selection, Appl. Numer. Math. 128 (2018) 139–156.
- [30] H. Liao, X. Song, T. Tang, T. Zhou, Analysis of the second-order BDF scheme with variable steps for the molecular beam epitaxial model without slope selection, Sci. China Math. 64 (5) (2021) 887–902.
- [31] L. Chen, J. Zhao, Y. Gong, A novel second-order scheme for the molecular beam epitaxy model with slope selection, Commun. Comput. Phys. 25 (4) (2019) 1024–1044.
- [32] M. Jiang, J. Zhao, Linear relaxation schemes for the Allen-Cahn-type and Cahn-Hilliard-type phase field models, Appl. Math. Lett. 137 (2023) 108477.
- [33] M. Jiang, Z. Zhang, J. Zhao, Improving the accuracy and consistency of the scalar auxiliary variable (SAV) method with relaxation, J. Comput. Phys. 456 (2022) 110954.
- [34] H. Liao, B. Ji, L. Zhang, An adaptive BDF2 implicit time-stepping method for the phase field crystal model, IMA J. Numer. Anal. 42 (1) (2021) 649-679.
- [35] X. Yang, D. Han, Linearly first- and second-order, unconditionally energy stable schemes for the phase field crystal model, J. Comput. Phys. 330 (2017) 1116-1134.
- [36] H.G. Lee, J. Kim, A simple and efficient finite difference method for the phase-field crystal equation on curved surfaces, Comput. Methods Appl. Mech. Eng. 307 (2016) 32–43.
- [37] J.-H. Park, A.J. Salgado, S.M. Wise, Benchmark computations of the phase field crystal and functionalized Cahn-Hilliard equations via fully implicit, Nesterov accelerated schemes, Commun. Comput. Phys. 33 (2023) 367–398.
- [38] D. Fan, L.Q. Chen, Computer simulation of grain growth using a continuum field model, Acta Mater. 45 (2) (1997) 611–622.
- [39] F. Boyer, C. Lapuerta, Study of a three component Cahn-Hilliard flow model, ESAIM: Math. Model. Numer. Anal. 40 (4) (2006) 653-687.
- [40] Y. Gong, Q. Hong, Q. Wang, Supplementary variable method for thermodynamically consistent partial differential equations, Comput. Methods Appl. Mech. Eng. 381 (2021) 113746.
- [41] Frédéric Hecht, New development in FreeFem++, J. Numer. Math. 20 (3-4) (2012) 251-266.